RESEARCH PAPER

Acta Neurobiol Exp 2024, 84: 1–25
DOI: 10.55782/ane-2024-2397

Optical imaging of the intrinsic signal as a tool to characterize orientation sensitivity in the primary visual cortex of the young mouse

Ida Raciborska[1,3*], Piotr Dzwiniel[2,3], Katarzyna Kordecka[2,3,4], Anna Posłuszny[3,4], Wioletta J. Waleszczyk[3†], Andrzej Wróbel[1,5]

[1] Laboratory of Neuroinformatics, Nencki Institute of Experimental Biology Polish Academy of Sciences, Warsaw, Poland
[2] Laboratory of Neurobiology of Emotions, Nencki Institute of Experimental Biology Polish Academy of Sciences, Warsaw, Poland
[3] Laboratory of Neurobiology of Vision, Nencki Institute of Experimental Biology Polish Academy of Sciences, Warsaw, Poland
[4] International Centre of Experimental Eye Research, Institute of Physical Chemistry Polish Academy of Sciences, Warsaw, Poland
[5] Department of Epistemology, Faculty of Philosophy, University of Warsaw, Warsaw, Poland
[†] Deceased on March 15th, 2020
** Email: i.raciborska@nencki.edu.pl*

We employed intrinsic signal optical imaging (ISOI) to investigate orientation sensitivity bias in the visual cortex of young mice. Optical signals were recorded in response to the moving light gratings stimulating ipsi-, contra- and binocular eye inputs. ISOI allowed visualization of cortical areas activated by gratings of specific orientation and temporal changes of light scatter during visual stimulation. These results confirmed ISOI as a reliable technique for imaging the activity of large populations of neurons in the mouse visual cortex. Our results revealed that the contralateral ocular input activated a larger area of the primary visual cortex than the ipsilateral input, and caused the highest response amplitudes of light scatter signals to all ocular inputs. Horizontal gratings moved in vertical orientation induced the most significant changes in light scatter when presented contralaterally and binocularly, surpassing stimulations by vertical or oblique gratings. These observations suggest dedicated integration mechanisms for the combined inputs from both eyes. We also explored the relationship between point luminance change (PLC) of grating stimuli and ISOI time courses under various orientations of movements of the gratings and ocular inputs, finding higher cross-correlation values for cardinal orientations and ipsilateral inputs. These findings suggested specific activation of different neuronal assemblies within the mouse's primary visual cortex by grating stimuli of the corresponding orientation. However, further investigations are needed to examine this summation hypothesis. Our study highlights the potential of optical imaging as a valuable tool for exploring functional-anatomical relationships in the mouse visual system.

Key words: mouse, visual cortex, orientation preference, cardinal bias, intrinsic signal optical imaging, visual evoked activation, oscillations

INTRODUCTION

The compiling of results from the various techniques of brain activity imaging (Hillman, 2007) has contributed to the understanding of the functional organization of the normal and malfunctioning cortex (Zepeda et al., 2004). Some of these techniques, such as two-photon imaging microscopy, calcium imaging or *in vivo* recording of electrical activity, have very good spatial and/or temporal resolution, but it could be challenging to use them for long-term observations lasting weeks or months. In addition, two-photon imaging and calcium imaging allow us to observe areas from 100-500 μm^2 (two-photon) to a few millimeters (calcium), which are

Received 30 July 2023, accepted 13 December 2023

much smaller than the areas imaged with intrinsic signal optical imaging (ISOI). Thus, these higher resolution methods allow us to delineate the extent of receptive fields of a single sensory cells and/or their functional assemblies, instead of the whole sensory projection area activated by its visual input and recorded by ISOI (Crowe & Ellis-Davies, 2014; Zepeda et al., 2004).

However, many studies have demonstrated that interactions and neuronal synchrony between all activated cortical regions are the basis for understanding the mechanisms of complex, long-lasting behavioral tasks (Jones & Barth, 1999; Rector et al., 2009; Jaramillo and Zador, 2014; Zhang et al., 2015; Chen et al., 2013). ISOI meets these requirements by allowing imaging of activation within the entire exposed cortical region with a spatial resolution of 50 – 100 μm (Grinvald et al., 1986; Lu et al., 2017; Ibbotson & Jung, 2020) and a temporal resolution of 100 ms (Frostig et al., 1990; Morone et al., 2017).

ISOI is also relatively non-invasive to rodents and easy to use in longitudinal studies and repetitive testing. At the same time, the ISOI signals closely correspond to activity measured by electrophysiological techniques, as demonstrated in the frog retina (Yao, 2009), barrel cortex (Rector et al., 2005), dorsal brainstem (Rector et al., 2001), and dorsal medulla of the rat (Rector et al., 1999), as well as in the visual cortex of cats and monkeys (Frostig et al., 1990).

The optical imaging of intrinsic activity is based on the spectral properties of hemoglobin, which absorbs more light when oxygenated and is therefore assumed to reflect increased neuronal activity (similar to near-infrared spectroscopy. Using a complementary metal-oxide-semiconductor (CMOS) camera as a photodetector array, this method measures light scatter (optical signal) that is proportional to the amount of oxygenated blood (intrinsic signal) (Fig. 1A–G and Fig. 2A) and thus related to neuronal activity (Raichle et al., 1976; Malonek & Grinvald, 1996; Frostig et al., 2006; Frostig & Chen-Bee, 2009).

Changes in light scatter related to neuronal activity are small, on the order of 1% of the measured signal amplitude (Morone et al., 2017). The absorption of oxygenated hemoglobin has two maxima, the first at 570 nm and the second at 605 nm. Interestingly, wavelengths below 550 nm can be used to visualize the mesh of blood vessels (Grinvald et al., 1986; Frostig et al., 1990). Therefore, in our setup, we used two separate wavelength filters to record changes in intrinsic optical properties of neural tissues, in particular light reflection, due to neuronal activity (605 nm – orange light) and blood vessels with oxygenated and deoxygenated blood (546 nm – "greenish" light) (Fig. 1A-C) (Frostig et al., 1990; Zepeda et al., 2004).

The ISOI method has already been used to study the activation of primary sensory cortical areas (Grinvald et al., 1999; Zepeda et al., 2004) and provided insights into the functional architecture of the visual cortex in monkeys, barrel cortex in rats (Sintsov et al., 2017), orientation columns in cats (Grinvald et al., 1986), and putative retinotopic organization in mice and cats (Schuett et al., 2002; Kalatsky & Stryker, 2003). However, it remains to be seen whether ISOI could be useful in studying cortical functionalities that are not represented by explicit cortical organization. For example, no specific, structural organization was confirmed to be responsible for the orientation-sensitive responses to visual stimuli in the mouse primary visual cortex (V1) (Hübener, 2003; Ohki & Reid, 2007; Gonzalo Cogno & Mato, 2015). The orientation-selective neurons are assumed to be randomly distributed over the whole V1 area (and referred to as "salt and pepper" structural organization) (Sohya et al., 2007; Niell & Stryker, 2008; Wang et al., 2010; Gonzalo Cogno & Mato, 2015). They constitute a large proportion of the cells in V1, ranging from 18% (Yoshida et al., 2012) to 39% (Bhaumik & Shah, 2014). Interestingly, Fahey and colleagues (2019), using a new technique for wide-field two-photon calcium imaging for collecting nearly the complete population of the cells' tuning preferences, argued for orientation bias around a single pinwheel centered in V1 of the mouse.

Until now, two-photon imaging and electrophysiology have been the most common *in vivo* strategies used to study orientation selectivity in mouse V1. These methods have revealed that the cortical visual areas activated binocularly by gratings of different orientations (moving orthogonally to the stimulus pattern) differ in size. For example, a study using sinusoidal grating moving back and forth with two-photon imaging (Yoshida et al., 2012) showed that the size of the activated cortical area was approximately two times larger during stimulation with horizontal (0/180°) than orthogonally oriented (90/270°) movements, despite similar densities of neurons that are sensitive to both orientations. Similarly, vertically oriented gratings presented binocularly evoked the largest visual cortical potentials (VEPs) in response to the horizontal direction of movements (Frenkel et al., 2006; Niell & Stryker, 2008).

In line with those results, single neurons sensitive to cardinal orientations in the mouse contralateral V1 showed a response twice as strong compared to neurons responding to oblique orientations of the moving gratings, as measured with two-photon imaging (Roth et al., 2012; Fahey et al., 2019), and similarly, the frequency of their spontaneous activity was twice as high (Wang et al., 2010). Interestingly, at the same time, orientation-sensitive neurons in the ipsilateral visual cor-

tex responded better to oblique gratings than those in contralateral V1 (Wang et al., 2010).

Previous experiments investigating the orientation preference of rodents using both behavioral and physiological methods have employed binocular visual stimulation. However, recent studies have shown that orientation sensitivity is also influenced by the ocular input. In binocular cells, the responses to contralateral eye stimulation are more orientation-selective than ipsilateral responses and strongly biased towards the cardinal orientations (Salinas et al., 2017). Wang and colleagues (2010) found that in young animals, binocular cells exhibit stronger responses to contra- and ipsilateral eye stimulation with cardinally orientated movements of gratings. Similarly, Salinas and colleagues (2017) observed a preference in binocular cells for cardinally oriented movements of gratings, but only for spatial frequencies higher than 0.24 cpd, while no preference was observed for ipsilateral input.

Most of the research on orientation tuning using the ISOI method in mice has focused on characterizing the cortical areas activated by visual stimulation while disregarding their temporal development and dependence on the type of peripheral inputs (Chapman et al., 1996; Rao et al., 1997; Kalatsky & Stryker, 2003; Cang et al., 2005; Yoshida et al., 2012; Pielecka-Fortuna et al., 2015). Therefore, a comprehensive understanding of the cortical origin of orientation sensitivity and its ocular determinants remains incomplete. It is important to investigate the possible interactions between different ocular components in the mechanism of orientation sensitivity, even though mice have laterally facing eyes (Ibbotson & Jung, 2020) and their cortical responses are dominated by the contralateral ocular input (Salinas et al., 2017; Scholl et al., 2017).

To find the basics of cortical orientation sensitivity, we analyzed in detail the dynamics of the intrinsic optical signal evoked in the right V1 by sinusoidal gratings moving in one direction perpendicularly to eight different orientations, i.e., 0°, 45°, 90°, 135°, 180°, 225°, 270°, 315° and presented *via* different ocular inputs (binocular, contralateral, and ipsilateral) for young mice (3-5 postnatal weeks) in which the visual cortex was already fully developed (Rochefort et al., 2011; Yoshida et al., 2012).

METHODS

Ethical approval

The experimental methods were performed in compliance with the guidelines provided by the Polish Academy of Sciences and carried out with the permission of the Local Ethical Commission No.1 in Warsaw (647/2014) and the European Community Council Directive (2010/63/UE).

Animals

C57BJ/6 male mice (n=9) aged 21-35 postnatal days (3-5 weeks) were used in this study. The mice were housed in groups of 4 or 5 and subjected to a reversed 12/12-hour light cycle. They had no prior history of participation in research studies. We employed male mice in the current study, as our laboratory traditionally utilizes male specimens for experimental procedures. This choice is based on the ready availability of male mice and allows for consistent comparisons of results within our research.

Surgical preparation

The animals were anesthetized in a chamber containing atmospheric air mixed with isoflurane (2-2.5%). Isoflurane remains a viable choice for ISOI studies (Constantinides et al., 2011; Yang et al., 2014). Most of the published research and our observations have highlighted the critical role of anesthetic concentration of isoflurane in achieving reliable and meaningful results. In general, maintaining a low concentration in the bloodstream produces stable hemodynamics and glucose metabolism with minimal impact on neural activity. Conversely, excessively high concentrations can compromise hemodynamics and make it impossible to obtain the correct ISOI signal. In our experiments, we consistently aimed to keep the isoflurane concentration as low as possible while ensuring adequate anesthesia.

When anesthesia had reached sufficient depth (the mouse did not react to tongue pulling), the animal was placed on a custom-made frame with ear bars holding its head with conical tips covered with 5% Lidocaine. During the surgical procedure, mouse anesthesia was maintained with 1.5-2% isoflurane mixed with oxygen *via* a gas mask placed on the nose (Fig. 1J). The animal's temperature was monitored and maintained with a heating pad at 36.5°C. The eyes were covered with a gel containing carbomer (2 mg/g) and then covered with opaque cotton pads to protect them from harsh light during the surgery. The pads were removed before the ISOI procedure.

The following substances were administered subcutaneously: Atropinum Sulfuricum (0.05 mg/kg b.w.), antibiotic 2.5% Baytril (5 mg/kg), and Dexamethasone (0.2 ml/kg b.w.). To anesthetize the tissue on the scalp, 2% Lidocaine (0.5 µl) was injected locally. The head skin

was cut, and the exposed skull was cleaned with saline and dried. As the mouse's skull is naturally highly transparent, it was not necessary to thin it, and the exposed bone was covered with agarose (solution of 114 mg agarose in 5 ml of NaCl) to maintain this transparency. This was placed on the scalp over the anatomical representation of the right visual field, covered with a 4 mm^2 glass coverslip, and protected with Vaseline to prevent drying out, following the protocol of Kalatsky and Stryker (2003) and Yoshida and colleagues (2012) (Fig. 1H). The level of isoflurane and exhaled gases (O_2 and CO_2) administered was monitored using a Datex Ohmeda Capnomac Ultima CO_2 Monitor, and an additional dose of isoflurane (20% of the initial dose) was given if needed. Fluids were administered subcutaneously using 0.9% NaCl solution and/or 5% glucose solution with 0.9% NaCl (2:1) in doses of 2 ml, every 2 hours alternately.

ISOI procedure and visual stimulation

The acute experiment was performed immediately after surgical preparation (no more than 20 minutes) in a darkened room, ensuring minimal auditory background noise. Intrinsic signals were recorded using a CMOS camera (Photon Focus MV1-D1312-160-CL-12), which has a maximum resolution of 1312 x 1082 pixels and uses a Nikkor 50 mm f/1.2 camera lenses with a pixel size of 8 x 8 µm. The camera was able to capture images of 3-4 mm^2 of the cortical surface. To illuminate the surface of the cortex, a 12V HAL lamp with an integrated thermal filter (KG1) was used, which was illuminated with two optical fibers and focusing lenses. The light then passed through the glass and agarose layers and the semi-transparent skull (Fig. 1D, H).

First, the area of interest was illuminated with a green light (546 nm) to capture an image of blood vessels in the skull and cortex. Based on this image, the position of the CMOS camera over the visual cortex area was set. Blood vessels visible in the green light were used as specific "signposts" (Fig. 1B, 1E, 1G).

Next, the focus of the camera was set to 450 µm below the cortical surface, covering the layers ranging from I to V, and the light was changed to orange (605 nm) to allow recording of the intrinsic signals in response to visual stimulus presentation (Fig. 1C, 1F, 1G). When imaging the brain, the CMOS camera records the reflected light as raw pixel intensity values, which are a digital representation of an analog signal converted by a digital-analog converter (DAC) (Fig. 2A). The pre-processing of the analog signal was determined by the implementation of the analog to digital software used for control of the Optical Imager 3001 system (Optical Imaging Inc., Rehovot, Israel).

The Optical Imager 3001 system (Optical Imaging Inc., Rehovot, Israel) (Heimel et al., 2007; Yoshida et al., 2012) controlled the CMOS camera and data recording. The ViSaGe MKII Stimulus Generator (Cambridge Research Systems, Rochester, UK) controlled the presentation of the visual stimuli, while a custom-written C# desktop application was responsible for defining their characteristics. All three components (the application, ViSaGe, and the Optical Imager) were interconnected and cooperated.

A NEC MultiSync FP2141SB CRT monitor with a resolution of 1024 x 768 pixels and a refresh rate of 120 Hz was placed 25 cm in front of the mouse (Fig. 1I). For monocular stimulations, the screen was moved by approximately 20° from the orthogonal axis while preserving the distance.

The visual stimuli consisted of black-and-white gratings of sinusoidal luminosity displayed on the whole screen and moving in one direction perpendicularly to eight different orientations: 0° moved from top to bottom, 45° from top left corner to bottom right corner, 90° from left to right, 135° from bottom left corner to top right corner, 180° from bottom to top, 225° from bottom right corner to top left corner, 270° from left to right, 315° from top right corner to bottom left corner (see Supplementary Fig. 1). Visual gratings had a spatial frequency of 0.05 cpd and a temporal frequency of approximately 1 Hz.

Additionally, homogeneous grey screens, referred to as 'blanks', with an average luminance between the black and white stripes of the grating, served as 'control' stimuli (Fig. 2D; blank I and blank II). Each trial lasted 9 seconds (Fig. 2C) and started with a blank presentation for 1 second (from time 0 to 1 s – blank I; Fig. 2D), followed by one of six randomly chosen stimuli (moving gratings of four different orientations and two blanks) lasting for 7 seconds (time 1-7 s). The trial ended with a repetition of the blank for 1 second (time between 8 and 9 s – blank II; Fig. 2D). The consecutive trials were separated by a 6-second presentation of another period of a blank screen during which the CMOS camera and HAL lamp illuminating the brain area with dual fiber optics were turned off. Six consecutive trials, each containing responses to one of the full sets of visual stimuli, formed a 'sub-block' (Fig. 2D), and 16 sub-blocks formed one 'block'. Each block was repeated for each ocular input, i.e., contralateral (left eye open, right eye covered with a light-proof slice), binocular (both eyes open), and ipsilateral (right eye open, left eye covered with a light-proof slice) (Fig. 2B, D), with a random order of the chosen ocular input. The optical imaging system recorded data (2D matrices of the light scatter values) with a sampling rate of 10 Hz (10 frames per second).

To investigate the time profile of PLC at the screen monitor during the movement of grating stimuli, we recorded signals from a photodiode placed at the center of the CRT using CED Spike 2 software (Cambridge Electronic Design, UK) with a signal sampling rate of 1000 Hz. Subsequently, we compared the PLCs with the time courses of matching optical signals through cross-correlation and phase shift calculations.

Data analysis

Data pre-processing and intrinsic signal time course generation

Offline data processing and analysis were conducted in MATLAB (MathWorks, Natick, MA) using the Optimage 1.1.7 toolbox (by Thomas Deneux, Unit of Neuroscience Information and Complexity, France). Fiji ImageJ

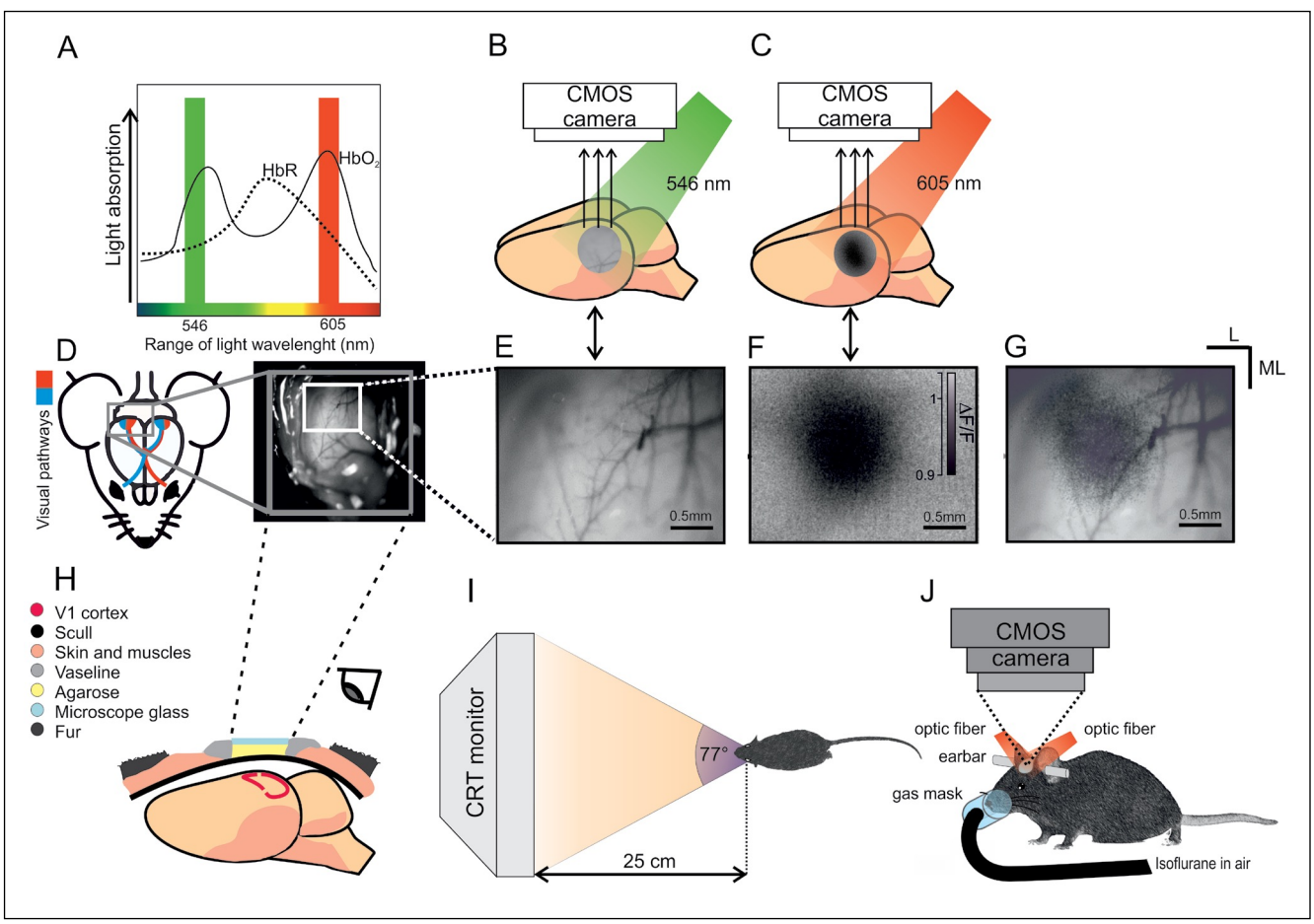

Fig. 1. Experimental setup for in vivo recording of stimulus-evoked intrinsic optical signal from the visual cortex. A. Light absorption spectra of non-oxygenated (HbR) and oxygenated hemoglobin (HbO_2) (Frostig et al., 1990). B. "Greenish" light (546 nm) was used to map blood vessels. C. Orange light (605 nm) was used to visualize cortical activity (hemoglobin oxygenation in the activated area). D. Left: simplified outline of the visual pathways of the mouse. Right: view of the right visual cortical area with brain surface and blood vessels. A white square delineates the area chosen for recording. E. Area of interest as seen by CMOS camera using 546 nm filter – dark ribbons represent cortical blood vessels. The camera was focused on blood vessels on the cortical surface. F. Area of interest as seen by CMOS camera when using a 605 nm filter – the darker the color, the higher the level of light scattering (absorption) and oxygenation of the hemoglobin in the blood (stronger neuronal activation). The camera was focused 450 µm below the cortical surface. The grey scale bar represents the light scatter change ΔF/F. G. Overlay of images shown in E and F. Images D, E, F, and G were taken from the same mouse. H. Cross section illustrates the scheme of the surgical preparation for the animal to the experiment. The skull (black) was unveiled above the right visual cortex (red). A layer of agarose (yellow) was applied to the skull and covered by a microscope glass (blue). Light exposures and recordings were conducted through all of the described layers. I. For binocular stimulation (field of view: vertical 61°, horizontal 77°), the distance between the animal nose placed perpendicularly to the CRT monitor was 25 cm. For monocular stimulations (contra- or ipsi), the screen was turned by 20° from the orthogonal axis with a preserved distance of 25 cm to the studied eye. J. The animal was anesthetized with 1.5-2% isoflurane mixed with air and placed on a custom-made frame, and immobilized with ear bars. The CMOS camera was set above the right visual cortex. The light passed a protective heat (infrared) filter and a 605 nm band-pass filter before being guided by a fiber optic to illuminate the cortex. Data collection and stimulus delivery were controlled by computers (not shown) controlled. See Methods for details.

(Schindelin et al., 2012) was also utilized, along with the triangular thresholding (Zack et al., 1977) and the JaCoP plugins (Bolte & Cordelières, 2006) for colocalization analysis. Custom Python scripts were developed to perform specific tasks related to data pre-processing, analysis, visualization, and statistical analysis. These tasks included comparing point luminance changes with intrinsic signal time courses for sinusoidal gratings of varied orientations and ocular input, assessing spectral characteristics of stimulus-induced changes of light scatter, and analyzing electrooculographic (EOG) signals recorded during anesthesia.

As described in section 2.4 (ISOI Procedure and Visual Stimulation), we recorded changes in light scat-

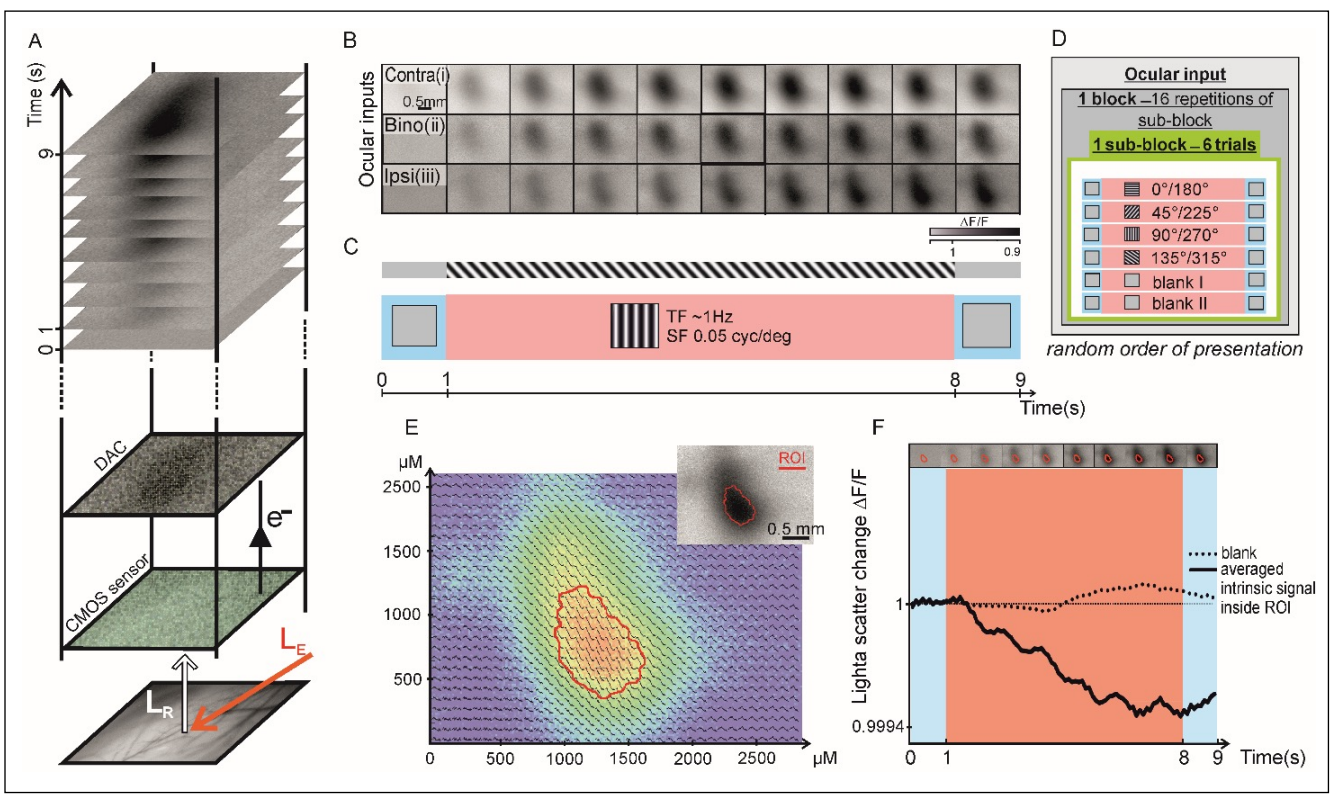

Fig. 2. Intrinsic signal optical imaging (ISOI) data pipeline used in the experiment. A. Scheme of the recording of the intrinsic signals. From the bottom: the cortical surface of the region of interest (ROI) imaged during the experiment. CMOS camera sensor (photodetector) detects changes in the light scatter across the cortical ROI (the difference between light emitted (L_E) by the optic fiber and the intensity of the light reflected to the camera sensor, L_R) and converts the detected light into a current (flow of the electrons e^-). The current flow (electrons accumulation proportional to the L_R) from within a cortical area of interest is converted by a digital-analog converter (DAC) into a brightness value of a single pixel being a part of a 1312 x 1082-pixel two-dimensional matrix saved on a computer's hard drive. Irradiation of the cortex to create one matrix lasted 1 s. The most upper stock: during 9 s of registration for a single trial (B, C), 90 2D matrices are collected with a sampling frequency of 10 Hz (for simplicity, only one 2D matrix is shown for 1 s of registration, i.e., 10 in total). B. The consecutive rows show dynamics of the cortical activation patterns in the right visual cortex evoked by visual stimulation for three different ocular inputs, i.e., contralateral (left eye open, right eye closed), binocular (both eyes open), ipsilateral (right eye open, left eye closed). The grey scale bar represents the change in light scatter ΔF/F. C. The sequence of visual stimulation in an exemplary trial with moving grating of vertical orientation. The trial lasts 9 s and consists of the presentation of the homogenous grey screen (0-1 s), the presentation of the sinusoidal grating of a given orientation and its movement in a specific direction (1-8 s), repetition of the presentation of the homogenous grey screen (8-9 s; 9 s in total). D. During the experiment, trials are organized in the following manner: six trials per 1 sub-block, 16 sub-blocks per 1 block, and blocks are repeated as many times as possible. One sub-block consists of 6 trials, with 4 being devoted to visual stimulation in the form of a sinusoidal grating in a specific orientation and moved in a specific direction, while the remaining two are devoted to the presentation of so-called "blanks" (I and II), which consisted only of a homogenous grey screen. Trials within sub-blocks are shuffled. Additionally, between each trial, a 6 s break is presented, which contains a homogenous grey screen as a "visual stimulus". E. The image of cortical activation patterns transformed into artificial colors with superimposed temporal profiles of stimulus-evoked signals (which correspond to appropriate pixels at the spatial matrix) of cortical activation registered during 9 seconds of recording, including horizontal grating stimulation *via* the ipsilateral eye. The averaged signal values from all pixels within the ROI (red line) were used to build up the temporal profile, as for Fig. 2F. After the recordings, we selected the ROI for each condition of the visual stimulation, which consisted of the area for which the brightness values were 10% below the maximum value (darker color à higher light scatter à stronger cortical activation). F. After averaging values of all pixels from the ROIs for a specific visual stimulation condition across 9 s of the recording, stimulus-evoked intrinsic signal time courses are calculated (solid black line). See Methods for details.

ter as two-dimensional arrays of pixels (1312 × 1082) with values represented on a brightness scale ("heat maps"). Higher levels of light scatter (light absorption) were represented by lower values of brightness, resulting in visually darker colors in specific portions of the recorded V1 area (Fig. 2A-C). ISOI data were collected throughout the entire 9-second trial, with experiments organized as follows: 1 block consisting of 16 sub-blocks, each containing 6 trials. Of these 6 trials, four were devoted to presenting a visual stimulus of a given orientation, while the remaining two trials were dedicated to presenting two blank screens labeled I and II (Fig. 2D).

After recording one block for each visual stimulus orientation and each blank, we obtained 16 × 90 matrices of light scatter data. The number of blocks we recorded depended on the animal's condition during the experiment, ranging from 1 to 4 blocks per ocular input. However, we aimed to ensure that each data set for a single animal and a given ocular input consisted of at least 2 blocks of recording. Therefore, for each animal and each ocular input, there could be 1-4 × 16 × 90 matrices of light scatter data.

To analyze the experimental outputs, we averaged the light scatter data for a specific animal, ocular input, block, and visual stimulus orientation (referred to as the "conditions") along the first axis, resulting in 90 x 2D matrices. Next, to determine the region of interest (ROI) with the highest cortex activation during visual stimulation for a given condition, we averaged 70 matrices within a trial range of 2-9 s (excluding blanks) into a single 2D matrix and defined the ROI (Fig. 2E). We then extrapolated the defined ROI backwards to the individual matrices within the given condition.

Next, the data was normalized into trial matrices within the ROI by dividing them by the signal from within the 0-1 s time period of the trial (homogeneous grey screen) and by the averaged blanks I and II, using the following formula:

$$\frac{\Delta F_{Ri}\ \frac{1}{\bar{x}F_{Si}}}{\Delta F_{Bi}}$$

Here, represents the values of light scatter changes recorded within 1-8 s of the trial, the specific visual stimulation represents the averaged values of light scatter changes recorded within 0-1 s of the trial with a uniform grey screen, and represents the values of light scatter changes recorded within 1-8 s of the averaged blank trials I and II. We subtracted the signal generated during 0-1 s from that generated during 1-8 s to eliminate any systemic components of non-stimulus-related signals. Dividing this difference by the signal during the blank stimulus recording was intended to further normalize the signal for stimulus-related neural responses. This method of signal normalization was used by Yoshida et al. (2012).

Finally, the resulting data, abbreviated as ΔF/F (relative light scatter change), were represented as a one-dimensional time course by averaging the values from within the ROI for each of the 90 matrices within a trial (as shown in Fig. 2F). Alternatively, data were represented as 2D matrices of values that represented cortical activation patterns (Fig. 2B, 2E).

Comparison of cortical activation patterns

The averaged data of intrinsic responses were exported from MATLAB Toolbox OptImage 1.1.7 to an 8-bit PNG heat map as a raster image file format (Fig. 3). A system of lossless compression of graphic data was used for each stimulus orientation in a sub-block. On the 8-bit PNG heat map, triangle thresholding was used to set a cut-off with brightness below 10% of the maximum value to create a so-called 'binary map' (black - activation, white - background/no activation, as delineated in Fig. 2E by the red line and shown in Fig. 3B-iii). Pixels within the ROI were then counted (Fig. 3C, D). For each animal, we calculated the mean size of the activated area in response to each presented stimulus and subjected the results to further statistical analysis.

Dynamics of stimulus-induced light scatter changes in time and space

The normalized data was exported from MATLAB Toolbox OptImage 1.1.7 for each data point of every stimulus orientation in a sub-block (Fig. 4). For each animal, we calculated the mean time course for each presented stimulus and subjected the results to further statistical analysis. We did not observe any significant differences in sizes of activated areas for different stimulus orientations or within the time courses for stimuli of the same spatial orientation but different directionality of movement (0° and 180°; 90° and 270°; 45° and 225°; 135° and 315°). Therefore, we decided to average them together (0°/180° as 0°; 90°/270° as 90°; 45°/225° as 45°; 135°/315° as 135°) for those animals for which we had presented orientations in both reciprocal directions (n=7; only n=2 mice were checked with visual stimuli of only 4 orientations / one direction 0°, 90°, 45°, 135°). However, we did not use averaged data from the response recorded in these two mice when checked in one direction for further analyzing the oscillations of the optical signals.

Measurements of PLCs and their comparisons with time courses of intrinsic signals for gratings of varied orientations and ocular input

To investigate PLC dynamics during the movement of a sinusoidal grating, we recorded signals from a photodiode placed at the center of the monitor using CED Spike 2 software (Cambridge Electronic Design, UK). The signal sampling rate was set to 1000 Hz (1000 frames per second) (see Supplementary Fig. 1), and we measured the change in luminance for sinusoidal gratings moving in one direction along four orientations: 0°, 45°, 90°, and 135°.

We compared the time courses of PLCs with those of matching stimulus-evoked intrinsic signals, using additional cross-correlation and phase shift calculations. This allowed us to initially verify potential oscillations in the optical signal time courses that were dependent on the movement of the sinusoidal grating for specific stimulus orientations and given ocular input. For more details on how the optical signal time courses were calculated, please refer to the section "Data pre-processing and intrinsic signal time course generation".

The cross-correlation coefficient between two signals X and Y, with a lag k, was defined as follows:

$$R(X,Y) = \sum_n X\,[n+k] \times \bar{Y}[n]$$

where and were the cross-correlated signals, was the number of samples, and was the complex conjugate of . The cross-correlation coefficient was then normalized and expressed in the range between -1 and 1. The lag between the two signals was expressed in seconds. The phase shift, represented in degrees, was defined as:

$$\Delta\varphi = \frac{360° \times k}{T}$$

where was the lag between two signals, and was the wave period, defined as:

$$T = \frac{1}{wave\ frequency\ (Hz)}$$

The pre-processing, analysis, and visualizations were performed using custom Python scripts.

Spectral characteristics of stimulus-induced light scatter changes

Given the clear pattern of PLC observed in response to the sinusoidal grating moving in one direction for a specific visual stimulus orientation, we investigated the possible spectral relationship between PLC and stimulus-induced light scatter change (ΔF/F) time courses. Specifically, we examined whether the time course of cortical activation in response to a moving visual stimulus of a given orientation contained an oscillating component related to the PLC pattern, with a frequency peak equal to 0.8571 Hz.

To achieve this, we calculated the stimulus-induced light scatter change (ΔF/F) time courses and their spectra for each ocular input and each orientation of moving gratings. Spectral analysis was performed using Discrete Fourier Transform (DFT; Cooley & Tukey, 1965) on the ΔF/F time courses.

Recording, processing and analysis of the EOG signal

To ascertain whether anesthetized mice follow bars moving on the screen with their eyes, we performed EOG signal recordings. We performed the recordings *via* two adhesive electrodes (GVB-geliMED, GmbH), correctly cut (5x5 mm) and glued to the shaved skin of the mouse above and below the eye. The signal was collected *via* CED Power1401 hardware and Spike2 software (Cambridge Electronic Design Limited), then processed, analyzed and visualized with custom scripts written in Python. The recordings were made for the entire experimental procedure, then divided into experimental conditions, averaged over the repetitions on the condition dimension and visualized in the form of time courses and frequency distributions.

Statistics

All signal values were reported as mean ± standard error of the mean (SEM), where applicable. The significance threshold was indicated by asterisks, where * denoted a p≤0.05, ** denoted a p≤0.01, and *** denoted a p≤0.001.

Statistical analysis of the activation areas was carried out using GraphPad Prism (version 8.1.4, GraphPad Software, La Jolla, California USA). Custom-written Python scripts were used to perform statistical analysis of stimulus-induced light scatter change (ΔF/F) time courses and their spectra. A significance threshold of p-values equal to 0.05 was assumed for all statistical analyses.

RESULTS

Different activation of V1 by moving gratings of different orientations and ocular inputs

We averaged the results of cortical activations measured for mice stimulated by gratings moved in both directions for each orientation (0°/180°; 90°/270°; 45°/225°; 135°/315°). The typical light scatter changes in the form of 2D images averaged for responses in reciprocal directions (Fig. 2B) representing the activated V1 areas by grating stimuli of different orientations are shown in Fig. 3A, B. Darker areas on the monochromatic images indicate higher light scatter change (i.e., stronger response), while a homogeneous grey background represents no evoked response within the stimulated regions (Fig. 2F; Fig. 3A).

We used Pearson's colocalization analysis to assess the extent of overlap for areas activated by gratings of different orientations for different types of ocular input. The areas of activation showed a high degree of similarity within the V1 region for consecutive orientations ($r \geq 0.92$) and for all ocular inputs ($r \geq 0.73$) (Fig. 3B).

It is important to note that the regional maps activated by the ISOI method are similar to consecutive stimulations but may differ when stimulated through different inputs. The upper panel on Fig. 3E recorded from an exemplary mouse shows different locations of the cortical areas activated by stripes moving along 45°/225° and 135°/315° orientations *via* contra- (upper left overlapping areas) and ipsi- (lower right overlapping areas) eye inputs. Moreover, the areas activated by moving stimuli of the same oblique orientations precisely overlap, while those activated by contralateral eyes differ within the whole sensory region. Thus, the cortical activation resulting from different stimulation paradigms results in a similar resolution to ISOI. Similarly, the lower panel of Fig. 3E shows a prominent difference between activity maps evoked by gratings moving along oblique orientations *via* ipsi and contra eyes for perpendicular cardinal orientations of strictly overlapping areas (45°/225° and 90°/270°).

We further compared the average number of pixels within ROIs (areas of cortical activations evoked by sinusoidal gratings of all orientations) depending on the type of visual input (binocular, contralateral, or ipsilateral) (Fig. 3C, Table 1). The Kruskal-Wallis test revealed a significant difference in the number of pixels within

Table 1. Summary of the descriptive statistics for the areas of activation and their scatter levels using the intrinsic signal. This is measured as light scatter changes caused by the oxygenated blood (ΔF/F) represented by values less than 1, whereas a value equal to 1 represents no changes in the light absorption. The summary contains statistics for all ocular inputs (ipsilateral, contralateral, binocular) and all grating orientations used in the study (0°, 45°, 90°, 135°, 180°, 225°, 270°, 315°, see Methods for details of presentation of visual stimuli). Data for grat ing orientations were paired, whereas the total number of mice contributing to a specific descriptive statistic sometimes differed between paired orientations due to the lack of the particular recording or due to unsatisfactory recording quality. Thus, n is expressed by two numbers corresponding to each movement direction of the same gratings' orientation pair.

	Stim. Or.	$MEAN_{area}$	SD_{area}	SEM_{area}	n_{area}	$MEAN_{ab.}$	$SD_{ab.}$	$SEM_{ab.}$	$n_{ab.}$
Ipsilateral	0°/180°	5960.6	2180.6	1327.6	9/6	0.999200	0.000117	0.000017	9/6
	45°/225°	6424.0	3699.7	1032.7	9/6	0.999163	0.000116	0.000016	9/6
	90°/270°	6148.5	3772.2	1579.4	9/6	0.999434	0.000082	0.000012	9/6
	135°/315°	6121.5	7777.2	676.2	9/6	0.999224	0.000091	0.000013	9/6
Contralateral	0°/180°	7462.1	3755.1	771.0	9/6	0.998857	0.000213	0.00003	9/6
	45°/225°	8588.4	2920.9	1308.0	9/7	0.998905	0.000182	0.000026	9/7
	90°/270°	8353.5	4178.7	1333.7	9/6	0.999007	0.000142	0.00002	9/6
	135°/315°	9931.7	1788.8	2749.6	9/6	0.998962	0.000147	0.000021	9/6
Binocular	0°/180°	7940.5	2973	1051.1	9/5	0.999047	0.000172	0.000024	9/5
	45°/225°	5981	4452.1	1574	9/6	0.999181	0.000172	0.000024	9/6
	90°/270°	7915.4	5296.3	1872.5	9/5	0.999179	0.000132	0.000019	9/5
	135°/315°	7513.7	5255.6	1858.1	9/5	0.999053	0.000146	0.000021	9/5

Stim. Or. – stimulus orientation. MEAN/SD/SEM/N_{area} – descriptive statistics for the areas of activation. MEAN/SD/SEM/$N_{ab.}$ – descriptive statistics for the light scatter change – light absorption. ab. - light absorption.

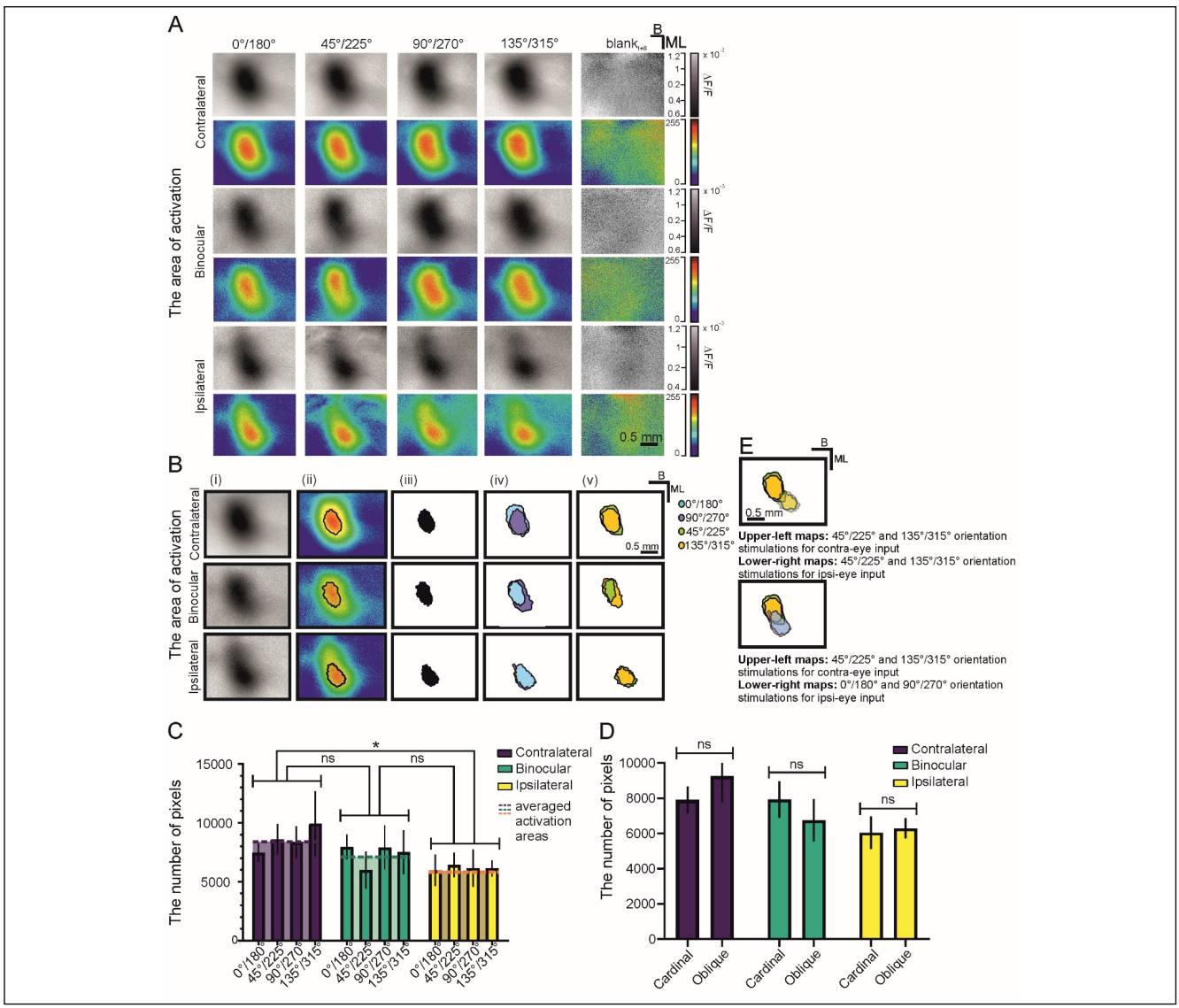

Fig. 3. Cortical activation patterns. A. Stimulus-evoked intrinsic signal maps for stimulation with a given orientation of grating and response to blank screens (I and II) recorded and averaged during stimulation in both directions *via* binocular, contralateral and ipsilateral ocular inputs. The value of each pixel building the map is the light scatter value. The grey scale bar values are normalized light scatter differences over baseline light scatter ΔF/F; the equivalent scale is values of arbitrary units of 8-bit PNG images from minimum (0) to maximum (255). How the signal is collected and converted to light scatter values and how the data is visualized in the form of maps and stimulus-evoked intrinsic signals of cortical activation are explained in the section regarding data analysis. B – bregma line; ML – midline. B. Cortical activation patterns were recorded from the exemplary mouse during visual stimulation with a grating of four specific orientations (two cardinal and two oblique). (i) Greyscale and (ii) heat scale maps representing responses to visual stimulation with gratings of horizontal orientation. (iii) Binary maps illustrating areas of the maximal cortical activation by the horizontal grating. (iv) Overlapped binary maps for two cardinal orientations (0°/180° and 90°/270°). (v) Overlapped binary maps for two oblique orientations (45°/225°, and 135°/315°). The separate analysis demonstrated a strong correlation between the overlapping areas (number of animals à n=9, Pearson's r>0.72, for details of presentation of visual stimuli, see Methods) (Table 3). C. Averaged (number of animals à n=9; for details of the presentation of visual stimuli, see Methods) number of pixels in the areas of activation by gratings of different orientations (narrow, colored bars) and ocular inputs (wide, light color bars). The only significant difference was found between the average number of pixels activated with stimulations *via* the contralateral (M=8583.9; SD=1021.1) and ipsilateral (M=6163.6; SD=192.4) eye (p=0.03, Kruskal-Wallis test, *post hoc* Bonferroni test). Error bars represent the standard error of the mean (SEM). D. Averaged (number of animals à n=9) number of pixels in the areas of activation during visual stimulation with gratings of cardinal (0°/180° and 90°/270°) and oblique (45°/225° and 135°/315°) orientations. No significant differences were found (p=0.06, $F_{(2,3)}$=5.3; two-way ANOVA test, *post hoc* Bonferroni test). E. Cortical activation patterns were recorded from the exemplary mouse during visual stimulation with a grating of four specific orientations (two cardinal and two oblique). Upper panel: superimposed activity maps for oblique orientation stimuli (45°/225° and 135°/315°) *via* contralateral and ipsilateral eye inputs. Lower panel: superimposed activity maps for stimulation along oblique orientation (45°/225° and 135°/315°) through the contralateral eye and activity maps for stimulation along cardinal orientation (0°/180° and 90°/270°) through the ipsilateral eye. Images in A, B and E come from the same animal. Error bars indicate SEM.

ROIs activated by contralateral and ipsilateral stimulation (p=0.03). Furthermore, post-hoc comparisons using the Bonferroni correction for multiple comparisons confirmed that the areas activated by contralateral stimulations (represented by the three wide, light color bars in Fig. 3C) differed from the areas activated by ipsilateral stimulations (p=0.01), whereas the areas activated by binocular stimulations were not significantly different from the other two.

Further analysis did not reveal any differences between ROIs activated by gratings of different orientations for either type of ocular input (p=0.06, $F_{(6,61)}$=0.8; two-way ANOVA test with Bonferroni *post hoc* test). Similarly, no differences were found between the areas activated by gratings moving in cardinal and oblique orientations for either type of ocular input (Fig. 3D).

Dynamics of light scatter change in V1 during stimulation by moving gratings with varied orientations and ocular inputs

Figs 4A and 4B display time courses of light scatter during stimulation by moving gratings of different orientations and a blank screen with a homogenous grey background. The increase in light scatter (decrease of recorded signal) was preceded by an initial dip (indicated by black arrows in Fig. 4B), similar to that observed in previous studies on rats, cats, monkeys and humans (recorded here as a positive increase in ΔF/F; Frostig & Chen-Bee, 2009; Hong & Zafar, 2018). During the 1-8 s time period, light scatter increased in response to the visual stimulation, resulting in a decreased ΔF/F signal (colored lines within the shaded area of Fig. 4A and 4B). When a blank screen was presented, the ΔF/F signal remained almost stable (black line in Fig. 4A and 4B). Notably, sinusoidal gratings with cardinal orientations produced signals with oscillating components that corresponded to the PLC frequency measured. However, this component was residual and negligible for oblique orientations of moving gratings (these findings are described in more detail in sections 3.3-3.5).

The Kruskal-Wallis test with *post hoc* Bonferroni test revealed significant differences (p<0.001) in the amplitudes of ΔF/F across all four movement orientations depending on the type of ocular input (contralateral, binocular, or ipsilateral). Contralateral visual stimulation induced the strongest light scatter changes (M=0.9991, SD=0.000399, $\Delta F/F_{MAX}$=0.9988) compared to both binocular (M=0.9993, SD=0.000337, $\Delta F/F_{MAX}$=0.9990) and ipsilateral trials (M=0.9994, SD=0.000263, $\Delta F/F_{MAX}$=0.9992) (Fig. 4C).

Further analysis also revealed that the mean values of light scatter changes (averaged within the time range 2-9 s of the trials) for sinusoidal grating stimuli of all orientations differed significantly depending on the ocular input used (p=0.01, $F_{(140,426)}$=1.37, two-way ANOVA test, *post hoc* Bonferroni test). Specifically, contralateral visual stimulation differed significantly from both binocular (p=0.001; df=283.0; t=28.29, posthoc Bonferroni test) and ipsilateral (p=0.001; df=283.0; t=52.98, *post hoc* Bonferroni test) stimulation. Moreover, binocular stimulation differed from ipsilateral stimulation (p=0.001; df=283.0; t=19.83, *post hoc* Bonferroni test) (Fig. 4D and Table 2).

To examine the differences in activation dynamics evoked by moving visual gratings across all ocular inputs regardless of stimulus orientation, we analyzed the time courses of stimulus-evoked light scatter changes (Fig. 4E). After measuring the differences at consecutive time points following the start of stimulations we found the first significant deviation of traces recorded for ipsilateral and contralateral ocular inputs at 2.4 s (p<0.01, *post hoc* Bonferroni test; indicated by the dotted vertical line labeled CI in Fig. 4E). The second significant deviation between traces obtained for contralateral and binocular ocular inputs occurred 3 s after start of the stimulation (p<0.01, *post hoc* Bonferroni test; indicated by the dotted line labeled CB in Fig. 4E). Finally, the third significant deviation of traces found between binocular and ipsilateral ocular inputs was observed at 4.5 seconds post-stimulus (p<0.05, *post hoc* Bonferroni test; indicated by the dotted line labeled BI in Fig. 4E). These observations suggest different inputs activate different sized areas of the visual cortex, with the largest effect observed for the contralateral input, followed by binocular input, and the smallest effect observed for ipsilaterally excited cells.

Additionally, we found that optical signals induced by contralateral, binocular, and ipsilateral visual stimulations exhibited high similarity, as indicated by the Pearson correlation coefficient analysis (r≤0.95) and differed significantly from the signal evoked by the blank screen (r=0) (Fig. 4F and Table 3).

Correlation between point luminance change of the grating and time course of stimulus-induced light scatter change

The time courses of PLCs recorded for gratings moved in all orientations had a similar oscillatory component of 0.8571 Hz. Cross-correlation analysis between PLCs and time courses of stimulus-induced light scatter changes (ΔF/F) revealed cardinal orientations

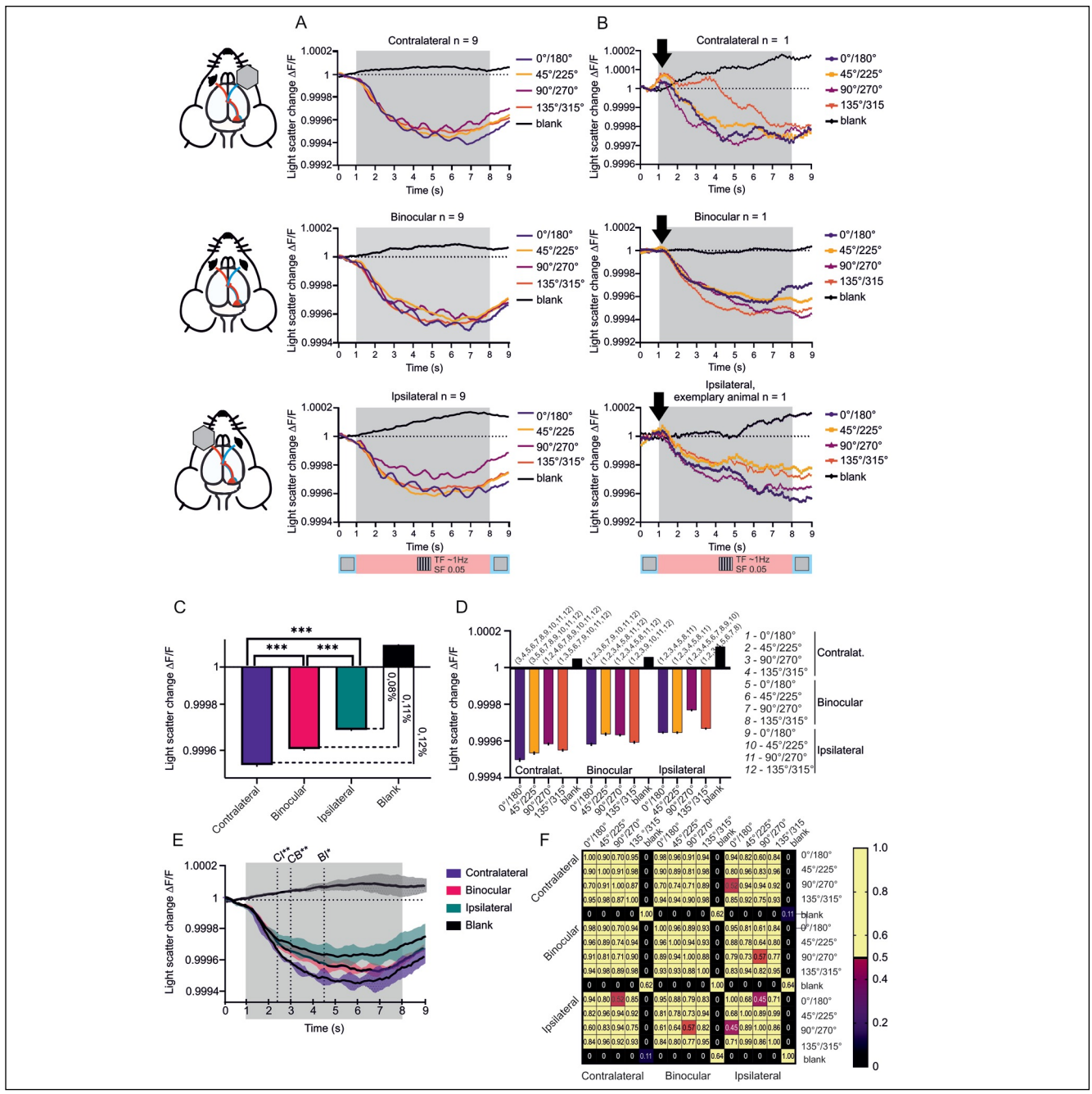

Fig. 4. Dynamics of stimulus-evoked intrinsic signals of cortical activation. A. Averaged (number of animals à n=9; for details of the presentation of visual stimuli, see Methods) values of the change in light scatter (ΔF/F) in response to moving gratings of different orientations and presentation of a blank screen recorded from an exemplary mouse. The recordings with different types of ocular input (contralateral, binocular, and ipsilateral) are shown in consecutive rows. B. Values of light scatter change (ΔF/F) recorded after a single visual stimulus presentation (one trial) from the same animal. The reversed initial dip is marked by a black arrow. The diagram below demonstrates the timing of screen patterns presentation during 9 s of stimulation. C. Averaged (number of animals à n=9) values of signals of the change in light scatter (ΔF/F) for 2-9 s of optical registration, for different options of visual stimulations; contralateral, binocular and ipsilateral compared to the light scatter changes value during the presentation of blank stimuli ($p<0.01$, df=2, Kruskal-Wallis test, *post hoc* Bonferroni test). The values (%) indicate a comparison of a light scatter change as a response to blank stimuli. D. Averaged values of signals of light scatter change (ΔF/F) (2-9 s of recording; number of animals n=9) for signals evoked by gratings of different orientations and types of ocular inputs. ($p=0.0004$, $F_{(140,486)}=1.54$ two-way ANOVA test, *post hoc* Bonferroni test) (Table 2). Error bars indicate SEM. E. Values of light scatter change (ΔF/F) for ocular inputs during 9 s recording with time points indicating the beginning of significant differences ($p<0.0001$, $F_{(118,360)}=5.988$ two-way ANOVA test, *post hoc* Bonferroni test) between signals recorded during stimulations *via* different inputs. CI – contralateral *vs.* ipsilateral; CB - contralateral *vs.* binocular; BI - binocular *vs.* ipsilateral. F. Matrix of signal correlations for grating stimuli of different orientations and blanks, on a Pearson's r scale from 0 (no linear correlation) to 1 (total positive linear correlation).

Table 2. Comparisons of the averaged light scatter changes for different types of ocular input (contralateral, binocular and ipsilateral) and different orientations of the moved grating (0°/180°, 45°/225°, 90°/270° and 135°/315°) for the 2-9 s time period. The table shows the results of the *post hoc* Bonferroni tests. Value notation: if $p \leq 0.05$ – *; if $p \leq 0.01$ – **; if $p \leq 0.001$ – ***; ns – no significant differences. The numbers in brackets refer to the column number in Fig. 4D.

		Contralateral				Binocular				Ipsilateral			
		(1) 0, 180	(2) 45, 225	(3) 90, 270	(4) 135, 315	(5) 0, 180	(6) 45, 225	(7) 90, 270	(8) 135, 315	(9) 0, 180	(10) 45, 225	(11) 90, 270	(12) 135, 315
Contralateral	(1) 0,180	–											
	(2) 45, 225	ns	–										
	(3) 90, 270	***	*	–									
	(4) 135, 315	**	ns	*	–								
Binocular	(1) 0, 180	***	***	ns	*	–							
	(2) 45, 225	***	***	***	***	***	–						
	(3) 90, 270	***	***	***	**	**	ns	–					
	(4) 135, 315	***	***	ns	**	ns	**	**	–				
Ipsilateral	(1) 0, 180	***	***	***	***	***	ns	ns	***	–			
	(2) 45, 225	***	***	***	***	**	ns	ns	*	ns	–		
	(3) 90, 270	***	***	***	***	***	***	***	***	***	***	–	
	(4) 135, 315	***	***	***	***	***	**	**	***	ns	ns	ns	–

Table 3. Pearson's average r for comparisons of matching location of 'binary images', for all types of visual stimulation, being contralateral, binocular and ipsilateral.

	Contralateral	Binocular	Ipsilateral
Contralateral	–	0.93	0.78
Binocular	0.93	–	0.73
Ipsilateral	0.78	0.73	–

produced the strongest co-occurrence of this oscillatory component, whereas it was negligible for the oblique orientations (Fig. 5 and Fig. 6). ISOI was also compared to the corresponding PLC time courses, as well as the cross-correlation between the signals for selected stimulus orientations and selected ocular inputs (Fig. 5). The strongest cross-correlation between the two signals was observed for ipsilateral stimulations at cardinal orientations (0°/180°, R_{MAX} (PLC, ΔF/F)=0.356, 90°/270°, R_{MAX} (PLC, ΔF/F)=0.207), and further, for binocular (0°/180°, R_{MAX} (PLC, ΔF/F)=0.219, 90°/270°, R_{MAX} (PLC, ΔF/F)=0.303) and contralateral (0°/180°, R_{MAX} (PLC, ΔF/F)=0.167, 90°/270°, R_{MAX} (PLC, ΔF/F)=0.103) ocular inputs, respectively. Interestingly, the ΔF/F time course for horizontal (0°/180°) orientations of moving grating was phase shifted about the corresponding PLCs by 0.5 s (154°) and for vertical (90°/270°) orientations by 0.1 s (31°) regardless of the choice of ocular input (see Fig. 5 for cross-correlations between PLC and ISOI time courses; see Fig. 6 for visualization of the maximal cross-correlations and calculated phase shifts between signals and Table 4 for more numerical details).

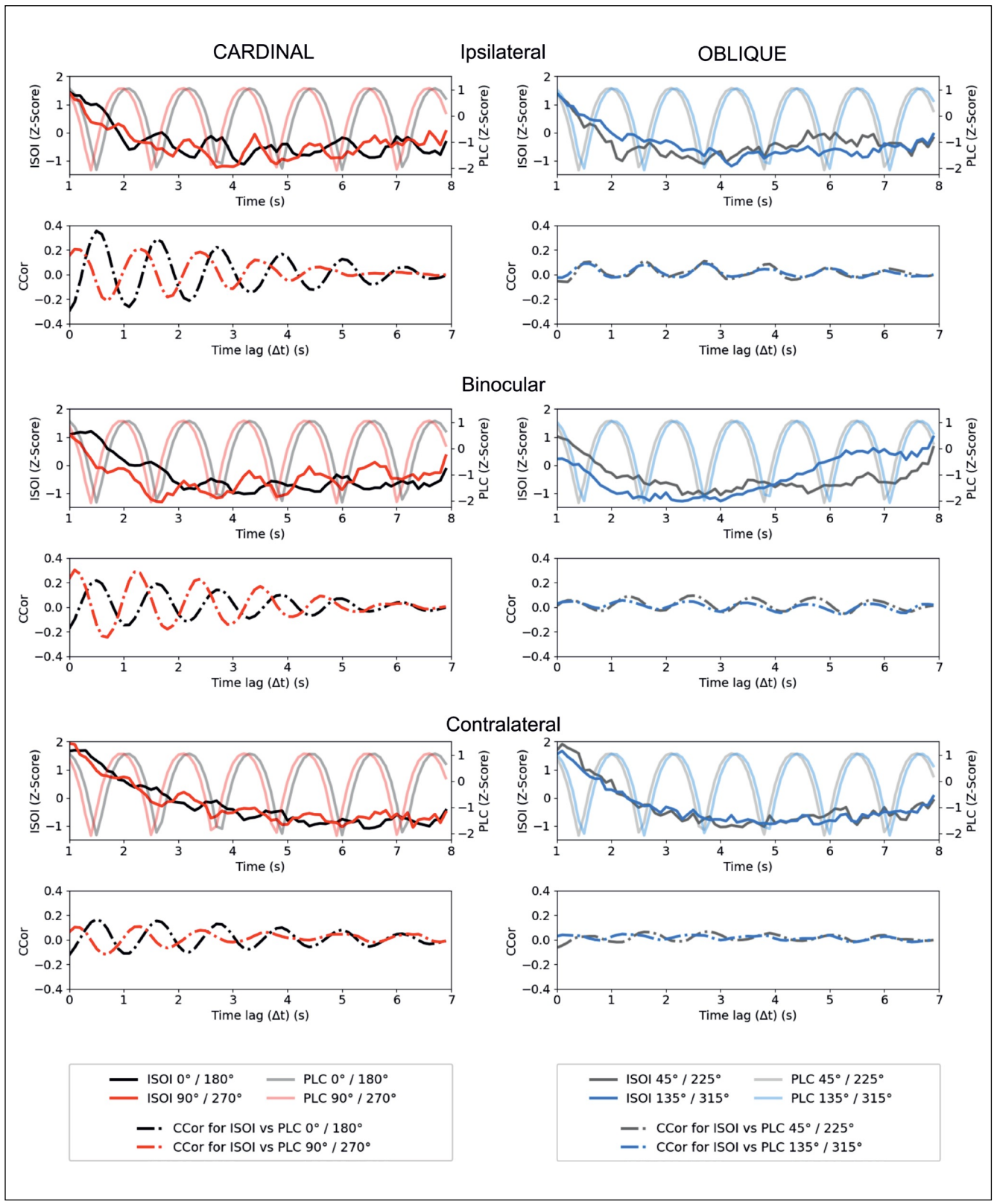

Fig. 5. Point luminance changes of a sinusoidal grating stimulus and its relation to time courses of intrinsic responses to movements along different orientations using cross-correlations. Cross-correlations (CCor) between point luminance change (PLC) and intrinsic signal optical imaging (ISOI) time courses were calculated and visualized for gratings moved along cardinal (left column; gratings 0°/180° and 90°/270°) and oblique (right column; gratings 45°/225°, and 135°/315°) orientations and for ipsilateral, binocular, and contralateral ocular inputs. ISOI time courses were averaged across animals (n=9).

Table 4. Cross-correlation maxima and phase shifts between PLC profiles of a particular stimulation grating and resulting time courses of light scatter changes (ΔF/F) for both cardinal and oblique orientation stimuli, and for all ocular inputs, i.e., ipsilateral, binocular and contralateral.

Ocular input	Orientation	Cross-Correlation	Phase Shift		
			(s)	(°)	(rad)
Ipsilateral	0°/180°	0.356	0.5	154	2.6878
	90°/270°	0.207	0.1	31	0.5411
	45°/225°	0.104	0.6	185	3.2289
	135°/315°	0.089	0.5	154	2.6878
Binocular	0°/180°	0.219	0.5	154	2.6878
	90°/270°	0.303	0.1	31	0.5411
	45°/225°	0.056	0.2	62	1.0821
	135°/315°	0.048	0.3	93	1.6232
Contralateral	0°/180°	0.167	0.5	154	2.6878
	90°/270°	0.103	0.1	31	0.5411
	45°/225°	0.029	0.6	185	3.2289
	135°/315°	0.041	0.1	31	0.5411

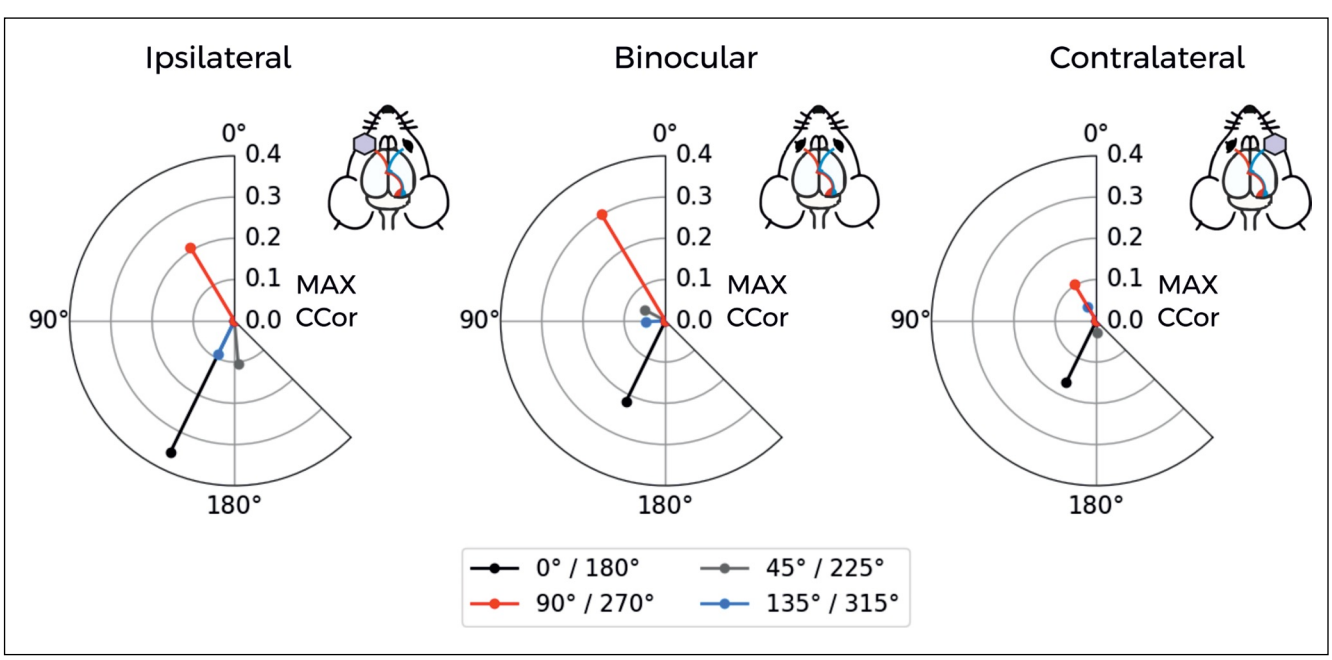

Fig. 6. Cross-correlation and phase shifts between point luminance changes (PLCs) of the grating stimulus and time course of stimulus-induced light scatter change. Phase shifts were calculated (and averaged over animals, ocular inputs, and grating orientation) for 7 s of the PLCs and ΔF/F time courses for cardinal (0°/180° and 90°/270°) and oblique (45°/225°, and 135°/315°) orientations of moving grating for all ocular inputs used in the experiment, i.e., ipsilateral, binocular, and contralateral. The radial axis represents values of the calculated cross-correlation (CCor) between PLCs and ΔF/F time courses (values between 0.0 and 0.4, the maximum value is indicated). The higher the cross-correlation value, the higher the level of co-occurrence of the PLC oscillatory component (0.8571 Hz) in the ΔF/F time course. The angular axis represents values of the calculated phase shift between PLCs and ΔF/F time courses (between 0° and 360°). A higher phase shift value characterizes a higher shift between the time course of ΔF/F and the PLC signal – 180° phase shift corresponds to 0.8571 Hz and 0.5833 s as the whole period lasts 1.1667 s.

Oscillatory characteristics of light scatter changes during stimulation by gratings of different orientations

The cross-correlations and phase shifts between PLCs and time courses of stimulus-induced light scatter changes (ΔF/F) indicated a relationship between visual stimulation by moving grating and the cortical response. Next, we calculated ΔF/F time course spectra for each type of ocular input and each grating orientation, taking into account data from mice stimulated by gratings that were moved in only one direction. Spectra here are defined as DFTs of the ΔF/F time courses. We found that ΔF/F time courses had the same main oscillatory component as the PLCs, i.e., 0.8571 Hz (Fig. 7). Interestingly, as initially suggested by cross-correlation and phase shift results, the highest peaks at this frequency were observed for stimuli that were moved along cardinal orientations (higher for horizontal compared to vertical orientation), whereas for oblique orientations, the oscillatory component was much less pronounced. Additionally, in contrast to the cross-correlation and phase shift results, the oscillatory components' power was highest for binoculars and lower for ipsilateral and contralateral ocular inputs, respectively.

We conducted statistical analyses to verify whether the oscillatory components of the ΔF/F time courses resulting from visual stimulation by gratings of the investigated orientations differ from the blank stimulus (Table 5). The highest calculated differences were observed for gratings moving along cardinal orientations (horizontal and then vertical), and once again, differences for oblique orientations were considerably lower. However, even the highest power of the oscillatory component observed for binocular input was not significantly different from the power evoked by the appearance of a blank stimulus. This could be due to the relatively small sample size, which was lower for the binocular than for the other ocular inputs, as well as the high variability of the ISOI time courses and their amplitudes across animals.

Notably, a one-way ANOVA performed for the dependent variable power and fixed factors ocular input and grating orientation revealed a significant effect of grating orientation ($F_{(8,115)}$=11.22, p<0.001, η^2=0.407).

EOG signal recorded during presentation of visual stimuli

Considering eye movements as a possible source of observed oscillations in the ISOI signal, we recorded the EOG signal during the presentation of visual stimuli for one mouse (Supplementary Fig. 2). We did

Table 5. Power measured for the 0.8571 Hz peak of the light scatter change time courses (ΔF/F) for all ocular inputs and orientations of grating with the one sample T-Test results and its significance represented by corresponding p-values. The T-Test statistic was performed between values obtained (for a given ocular input) during stimulation by grating of specific orientation and blank, whereas the mean of the blank values was treated as a populational mean of the one sample T-Test.

	Ocular Input and Statistics	0°	45°	90°	135°	180°	225°	270°	315°
Ipsilateral	POWER	5.2679	2.5904	3.6500	2.4885	4.9910	3.1146	2.5465	2.6102
	T-STAT	2.8267	2.1632	2.6682	1.3821	2.5400	1.5098	2.0394	1.2523
	P-VAL	0.0301	0.0738	0.0371	0.2162	0.0519	0.1915	0.0969	0.2659
	SIG	*	n.s.	*	n.s.	n.s.	n.s.	n.s.	n.s.
Binocular	POWER	5.5606	3.0932	4.9226	3.2947	5.8367	2.6960	3.7219	2.9067
	T-STAT	1.7641	0.8810	2.0866	1.0981	2.0187	0.4853	2.1239	0.7547
	P-VAL	0.1380	0.4186	0.0913	0.3222	0.1137	0.6480	0.1009	0.4924
	SIG	n.s.	n.s.	n.s.	n.s.	n.s.	n.s.	n.s.	n.s.
Contralateral	POWER	4.6188	2.7906	4.0744	1.9437	5.8543	3.1492	3.2006	3.1291
	T-STAT	2.4793	1.2981	3.0378	2.0154	2.7060	2.2940	3.5367	1.7225
	P-VAL	0.0479	0.2419	0.0229	0.0905	0.0425	0.0616	0.0166	0.1456
	SIG	*	n.s.	*	n.s.	*	n.s.	*	n.s.

A single asterisk (*) represents for p-value < 0.05, whereas "n.s." represents p-values >= 0.05.

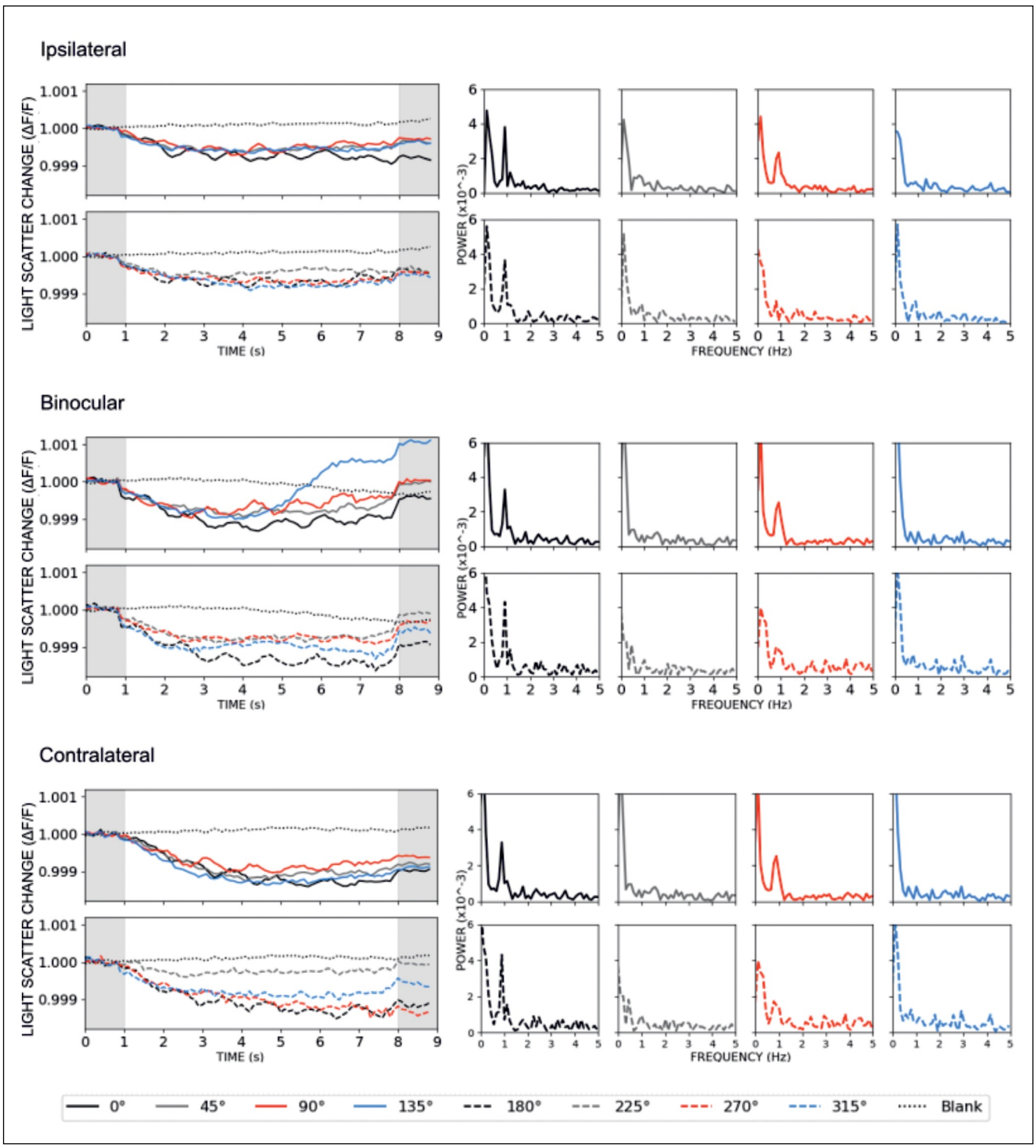

Fig. 7. Time courses of light scatter change induced by visual stimuli and their frequency spectra evoked through contra-, ipsi- and binocular ocular input types and different grating orientations. Experimental design assumed the presentation of a whole-screen sinusoidal grating moved along four specific orientations, each with two reciprocal directions (0° and 180°, 45° and 225°, 90° and 270°, 135° and 315°), with a fixed moving speed (0.8571 Hz; measured by a photodiode). These stimuli were presented *via* three specific ocular input types (ipsilateral, contralateral, and binocular). Each recording lasted 9 s, whereas each stimulus presentation lasted 7 s and was preceded and followed by a 1 s display of a homogenous grey background (blank indicated by grey areas on the first column plots). Cortical activation was also recorded during the 7 s presentation of the sole homogenous grey screen (blank). Optical signal responses in the form of time courses of stimulus-evoked changes in light scatter (ΔF/F) for a specific ocular input type and grating orientation are presented on the left side of the figure. The individual spectra of each time course were calculated using Discrete Fourier Transform (DFT) and plotted on the right side of the figure within 0.1-5.0 Hz frequency range and 0-6 ($\times 10^{-3}$) power.

not observe any relationship between EOG and PLC signals. The time course of the EOG signal regardless of the experimental condition (BLANK I/II or presentation of moving sinusoidal gratings along different orientations, i.e., 0°/180°, 45°/225°, 90°/270°, and 135°/315°, similar as in the main experiment) was random with no apparent relationship to visual stimulation. Similarly, the frequency distributions were random and did not demonstrate the 0.8571 Hz component of the PLC frequency that is seen in the ISOI signals that were recorded during the presentation of cardinal stimuli.

DISCUSSION

In this study, we have confirmed previous data that ISOI is a valuable method for studying the evoked activity within the primary visual cortex of mice (e.g., Kalatsky & Stryker, 2003; Yoshida et al., 2012; Kondo et al., 2016) and specifically, the cortical orientation sensitivity evoked by sinusoidal moving gratings (e.g., Yoshida et al., 2012). Additionally, we investigated for the first time changes in the optic signal strength over time. Specifically, ISOI enabled the study of the dynamics of light scatter changes elicited by moving gratings, which were found to vary across different orientations and ocular inputs (binocular, contralateral, and ipsilateral). The responses to gratings moved along cardinal orientations, but not along oblique orientations, and were characterized by optical signal oscillations at the spatial frequency of the grating. These differences could reflect the mechanisms of summation within the putative, specific orientation assemblies within the primary visual cortex and thus were a valuable tool for investigating functional-anatomical relationships within the mouse visual cortex. The results presented in this paper provide evidence for the existence of a functional microsystem composed of cells that behave like those cells within organized neuronal assemblies, that are sensitive to specific orientations, and that interact with each other during the presentation of orientation stimuli. This hypothesis could be addressed with future studies on this topic.

Impact of ocular input type on light scatter changes in primary visual cortex

We found that stimulation *via* different ocular inputs resulted in the activation of different portions of the cortical tissue, with contralateral input activating the largest area of the visual cortex and ipsilateral input activating the smallest area (difference of 39.2%). These changes were most pronounced in the amplitude of the light scatter signals, with the largest change observed after contralateral stimulation, followed by smaller changes evoked by bilateral and ipsilateral stimulations.

These findings are consistent with previous reports indicating that only 5% of cells in the visual cortex are driven exclusively by ipsilateral eye input, while contralateral eye stimulation drives 95% of orientation-sensitive cells and activates the greatest cortical area (Dräger, 1975; Mangini & Pearlman, 1980; Wagor et al., 1980; Métin et al., 1988; Hübener 2003). Furthermore, it was found that 70% of cells activated by contralateral input were also driven binocularly (Métin et al., 1988). These results support the notion that contralateral ocular input reaches a larger number of cells, thereby activating a greater cortical region than binocular and ipsilateral inputs (Pielecka-Fortuna et al., 2015; Salinas et al., 2017; Hong et al., 2020).

Binocular input is required to reveal cardinal bias in activation areas

Although the mouse cortex is often described as unstructured and its organization referred to as "salt-and-pepper", recent studies have shown some degree of functional organization (Hübener, 2003; Skyberg et al., 2020). We did not find significant differences in response characteristics between cardinal (horizontal 0°/180° and vertical 90°/270°) and oblique (45°/225°; 135°/315°) orientations of moving gratings presented via different ocular input types. While it is generally agreed that responses in V1 for cardinal and oblique orientations differ (Tan et al., 2011; Salinas et al., 2017), our statistics showed differences only at p=0.06. However, it should be noted that p values in the region of 0.05 represent modest degrees of evidence, regardless of which side of the division they lie on (Wood et al., 2014).

Then, in a similar manner to previous studies, we confirmed the presence of the "oblique effect" during binocular stimulation (14.89% difference in the area of activation between cardinal and oblique orientations, as shown in Fig. 3C and Fig. 3D) similar to previous studies (Appelle, 1972; Coppola et al., 1998; Li et al., 2003).

The result of the cardinal bias found in our experiment for binocular stimulation agrees with previous electrophysiological (Valois et al., 1982; Kreile et al., 2011) and two-photon imaging studies (Kreile et al., 2011; Yoshida et al., 2012), in which cortical cells were

shown to react strongly to visual stimulation in cardinal compared to oblique orientations. This is likely due to more cells being sensitive to gratings moved in a cardinal direction (Li et al., 2003). Interestingly, when visual stimuli were delivered simultaneously but separately to each eye, the effect of cardinal stimulus preference disappeared (Blake & Holopigian, 1985; De Weerd et al.,1990) or, if stimuli were complex, the "oblique effect" was reversed (Essock et al., 2003). Thus, our results add new but matching data on the relation of orientation selectivity from ocular input type. Moreover, our data confirms that ISOI could be used in future longitudinal studies on computational mechanisms in the mouse visual cortex.

Evidence of horizontal bias for contralateral visual stimulation through analysis of light scatter change courses

The changes in light scatter demonstrated the usefulness of the ISOI recording method used in this study for the investigation of orientation selectivity mechanisms in the visual cortex of mice. Our study demonstrated (i) the contralateral ocular input elicited the strongest light-scatter changes and thus, on average, the highest activation of neuronal populations ($p<0.01$); (ii) for each of the ocular inputs utilized, the mouse visual cortex was most sensitive to horizontal gratings (0°/180°) moved in a vertical orientation when compared to movements in other presented orientations ($p=0.0004$); (iii) the specific orientation networks of cortical cells might result in different activity patterns, as indicated by the dynamics of light-scatter changes, which were statistically distinct from each other (Table 2).

Previous electrophysiological single-unit recordings and two-photon imaging in adult mice (Kreile et al., 2011; Yoshida et al., 2012) found the strongest responses (more spikes or activated cells during imaging) to horizontal gratings (0°/180°) that were moved vertically (up and down) compared to oblique gratings (45°/135°/225°/315°) moved in perpendicular orientations. Our study obtained similar results (Fig. 4A and Fig. 4D), observing that horizontal movements of vertical gratings (90°/270°) caused the smallest light scatter changes (Fig. 4A and Fig. 4D). These findings were comparable to those observed for control groups in both of the previous experiments (Kreile et al., 2011; Yoshida et al., 2012), as well as in a group of juvenile mice (Wang et al., 2010).

It is worth noting that studies using visual stimuli with similar physical properties to those used in our experiment also yield comparable results (Niell & Stryker, 2008). However, changing the physical properties of the stimulus can lead to opposite results, as shown in Zhao et al. (2013) and Ayzenshtat et al. (2016), where vertical gratings were the more preferred. Therefore, further research is needed to better understand these complexities.

Grating-related oscillations of light scatter changes in V1 and their relationship to cardinal orientations and ocular input type

We typically observed oscillations of the light scatter changes over the V1 area that were related to the stimulations by sinusoidal gratings. The frequency of these oscillations was identical to the PLCs measured at the central point of the screen. These oscillations were strongest in signals recorded in response to gratings in cardinal orientations, with a greater effect caused by horizontal (0°/180°) compared to vertical (90°/270°) orientations. Interestingly, the oscillations evoked by vertical gratings moved along the horizontal orientation were in phase with the PLC (90°/270°), while the horizontal gratings moved along vertical orientations (0°/180°) caused responses in the opposite phase (Fig. 5, left column). Importantly, discussing the results regarding the observed phase shifts is difficult due to the characteristics of the ISOI signal and the low signal sampling frequency. Nevertheless, we found that these oscillations occurred regardless of the type of ocular input, whether it was *via* the ipsi- or contralateral eye, or by binocular vision. As the frequency of the intrinsic signal oscillations was identical to PLCs of grating stimuli, it was likely that they resulted from the summation of transient responses of groups of cells (Perry & Fallah, 2014) that reacted most strongly to gratings moved in cardinal orientations (Weiler et al., 2022; Scholl et al., 2022).

The other possible oscillatory input to V1 could involve recurrent activation *via* the motor system (Straka et al., 2018; Parker et al., 2020). It is well known that the processing of sensory information involves modulatory input from the motor cortex (Belooze-rova et al., 2010; Niell & Stryker, 2010; Farrell et al., 2015; Heindorf et al., 2018; Murty et al., 2018). However, we excluded the possibility that the recorded ISOI oscillations were the result of eye movements following the visual stimuli based on the lack of any specific frequency component in the EOG signal associated with visual stimuli. Here, we are primarily referring to the main frequency component of the PLC signal, namely the 0.8571 Hz observed in the ISOI signal for cardinal stimuli, and not present in recordings for oblique stimuli and in the EOG signal. It is import-

ant to emphasize that the EOG signal recordings were performed only in one mouse.

Thus, the oscillatory components of the intrinsic signals most likely reflected the computation of exogenous signals in different parts of the V1 networks according to their structural/functional basis. Admittedly, the resolution of ISOI does not allow for the activity recording of single cells, but is sufficient to record the summed activity of cell assemblies consecutively excited by visual stimuli moved along cardinal orientations (similar results were obtained by Zhang et al. (2018) and Craddock et al. (2023). Thus, the observed ISOI oscillations evoked by stimuli moving vertically or horizontally would reflect the summation within functional networks spread over V1 and adjacent structures (Polack & Contreras, 2012). Recent studies revealed that neuronal oscillations play a crucial role in coordinating input and output states within networks of macro columns for fine-scale integrated processing (Bennett, 2020; da Costa & Martin, 2010; Laberge & Kasevich, 2017; Ringach et al., 2016). In the mouse visual cortex, several researchers have demonstrated a significant decrease in tuning similarity with cortical distance, indicating spatial clustering. Additionally, evidence of neuronal clustering at various cortical depths aligns with columnar organization, implying a structured local layout (Ringach et al., 2016). The recent papers of Laberge and Kasevich (2017) and Bennett (2020) also support the idea that fine-tuned cells in macro- and micro-columns receive coded pulse trains from each other amplified by specific oscillation frequencies, acting as a bidirectional interneuronal communication channel.

In higher mammalian species, cells with affection for a specific orientation have also clustered into macro-recognizable structures (orientation regions), which are represented by so-called retinotopic maps. It is generally agreed that, in mice, cells are not spatially organized as in higher mammals, rather they exhibit a salt-n-paper spatial distribution of neurons with given orientation specificity. However, according to our hypothesis, at the same time, the orientation selective cells interconnect into specific functional assemblies (orientation networks). This, in turn, can be reflected in the observed oscillations resulting from vertically and horizontally moving gratings, which have their explicit retinotopic representation (Polack & Contreras, 2012; Perry & Fallah, 2014). Additionally, given the ability of weak endogenous electric fields to amplify and synchronize neocortical network activity (Fröhlich & McCormick, 2010), the oscillations for cardinal stimuli have the potential to enhance functions related to visual information processing related to these stimuli. Conversely, the oblique stimuli can induce the activation of both networks at once. Given their retinotopy for horizontal and vertical stimuli reflected in the ΔF/F time courses as opposite-phase oscillations, this may contribute to the apparent nulling of oscillations from the recording's perspective while processing information on oblique stimuli. Nevertheless, recent studies have shown that reality can be far more complex than we have assumed so far in the discussion, and visual stimulus preferences most likely have their source in a multiregional functional recurrent communication between many cortical and subcortical modules processing information simultaneously, rather than in a point-to-point manner as in the classical approaches (Rossi et al., 2020; Weiler et al., 2022; Jia et al., 2022; Scholl et al., 2022).

Classically, the selectivity for oriented visual stimuli could be "sorted out" by simple cells in visual cortex layer IV *via* the convergence of ON-center and OFF-center thalamic inputs whose receptive fields are offset in visual space, but are lacking orientation selectivity (Hubel & Wiesel, 1962). This mechanism implies preferential connectivity between neurons responding to the same stimulus orientation in layer IV, suggesting the existence of a structural-functional neural network "tuned" for the processing of visual stimuli containing well-defined spatiotemporal characteristics (Lien & Scanziani, 2013; Freeman, 2021). Moreover, this also suggests that a responsible neural network may also be wired for the relative positions of ON and OFF fields/domains (i.e., phase of the stimuli), resulting in different phase modulation of intracortical excitation by sinusoidal moving grating of variable orientation.

Summarizing all of these issues, we presume that there could be more than one mechanism contributing to the observed ISOI ΔF/F time course oscillations for cardinal orientations and the lack of such for oblique orientations. Firstly, there could be a simple summation of the transient cell activity that responds most strongly to the moving visual stimuli of cardinal orientations, in both the visual thalamus and cortex. Secondly, there could be a synchronization of cells that constitute a specialized network reflecting a preference for cardinally oriented stimuli – separately for horizontal and vertical orientation, as shown on the retinotopic maps by Polack and Contreras (2012). Thirdly, there may be activation of both of these networks during stimulation with oblique-oriented stimuli. While ISOI is an interesting method for observing oscillations for slow-moving stimuli, a closer follow-up examination of our results would require a technique with higher temporal resolution, such as VSD and/or multi-electrode ECoG surface recordings.

ACKNOWLEDGMENTS

This work was supported by the National Science Centre grants 2013/08/W/NZ4/00691 and 2016/23/N/HS6/02346.

REFERENCES

Appelle S. (1972) Perception and discrimination as a function of stimulus orientation: the "oblique effect" in man and animals. *Psychological bulletin*, *78*(4), 266–278. https://doi.org/10.1037/h0033117

Ayzenshtat, I., Jackson, J., & Yuste, R. (2016) Orientation tuning depends on spatial frequency in mouse visual cortex. *eNeuro*, *3*(5), ENEURO.0217-16.2016. https://doi.org/10.1523/ENEURO.0217-16.2016

Beloozerova, I. N., Farrell, B. J., Sirota, M. G., & Prilutsky, B. I. (2010) Differences in movement mechanics, electromyographic, and motor cortex activity between accurate and nonaccurate stepping. Journal of neurophysiology, 103(4), 2285–2300. https://doi.org/10.1152/jn.00360.2009

Bennett, M. (2020) An attempt at a unified theory of the neocortical microcircuit in sensory cortex. Frontiers in Neural Circuits, 14(July), 1–32. https://doi.org/10.3389/fncir.2020.00040

Bhaumik, B., & Shah, N. P. (2014) Development and matching of binocular orientation preference in mouse V1. *Frontiers in systems neuroscience*, *8*, 128. https://doi.org/10.3389/fnsys.2014.00128

Blake, R., & Holopigian, K. (1985) Orientation selectivity in cats and humans assessed by masking. *Vision research*, *25*(10), 1459–1467. https://doi.org/10.1016/0042-6989(85)90224-x

Bolte, S., & Cordelières, F. P. (2006) A guided tour into subcellular colocalization analysis in light microscopy. *Journal of microscopy*, *224*(Pt 3), 213–232. https://doi.org/10.1111/j.1365-2818.2006.01706.x

Cang, J., Kalatsky, V. A., Löwel, S., & Stryker, M. P. (2005) Optical imaging of the intrinsic signal as a measure of cortical plasticity in the mouse. *Visual neuroscience*, *22*(5), 685–691. https://doi.org/10.1017/S0952523805225178

Chapman, B., Stryker, M.P., & Bonhoeffer, T. (1996) Development of orientation preference maps in ferret primary visual cortex. *Journal of neuroscience*, 16(20), 6443–6453. https://doi.org/10.1523/JNEUROSCI.16-20-06443.1996

Chen, T. W., Wardill, T. J., Sun, Y., Pulver, S. R., Renninger, S. L., Baohan, A., Schreiter, E. R., Kerr, R. A., Orger, M. B., Jayaraman, V., Looger, L. L., Svoboda, K., & Kim, D. S. (2013) Ultrasensitive fluorescent proteins for imaging neuronal activity. *Nature*, *499*(7458), 295–300. https://doi.org/10.1038/nature12354

Constantinides, C., Mean, R., & Janssen, B. J. (2011) Effects of isoflurane anesthesia on the cardiovascular function of the C57BL/6 mouse. ILAR Journal / National Research Council, Institute of Laboratory Animal Resources, 52(3), e21–e31.

Craddock, R., Vasalauskaite, A., Ranson, A., & Sengpiel, F. (2023) Experience dependent plasticity of higher visual cortical areas in the mouse. Cerebral Cortex, 33(15), 9303–9312. https://doi.org/10.1093/cercor/bhad203

Crowe, S. E., & Ellis-Davies, G. C. R. (2014) Longitudinal in vivo two-photon fluorescence imaging. Journal of Comparative Neurology, 522(8), 1708–1727. https://doi.org/10.1002/cne.23502

Good, I.J. (1997) Introduction to Cooley and Tukey (1965) An Algorithm for the Machine Calculation of Complex Fourier Series. In: Kotz, S., Johnson, N.L. (eds) *Breakthroughs in Statistics. Springer Series in Statistics*. Springer, New York, NY. https://doi.org/10.1007/978-1-4612-0667-5_9

Coppola, D. M., Purves, H. R., McCoy, A. N., & Purves, D. (1998) The distribution of oriented contours in the real world. *Proceedings of the National Academy of Sciences of the United States of America*, *95*(7), 4002–4006. https://doi.org/10.1073/pnas.95.7.4002

Da Costa, N. M., & Martin, K. A. C. (2010) Whose cortical column would that be? Frontiers in Neuroanatomy, 4, 16. https://doi.org/10.3389/fnana.2010.00016

Dräger U. C. (1975) Receptive fields of single cells and topography in mouse visual cortex. *The Journal of comparative neurology*, *160*(3), 269–290. https://doi.org/10.1002/cne.901600302

Essock, E. A., DeFord, J. K., Hansen, B. C., & Sinai, M. J. (2003) Oblique stimuli are seen best (not worst!) in naturalistic broad-band stimuli: a horizontal effect. *Vision research*, *43*(12), 1329–1335. https://doi.org/10.1016/s0042-6989(03)00142-1

Fahey P.G., Muhammad T., Smith C., Froudarakis E., Cobos E., Fu J., Walker E.Y., Yatsenko D., Sinz F.H., Reimer J. & Tolias A.S. (2019) A global map of orientation tuning in mouse visual cortex. *bioRxiv* 745323; doi: https://doi.org/10.1101/745323

Farrell, B. J., Bulgakova, M. A., Sirota, M. G., Prilutsky, B. I., & Beloozerova, I. N. (2015) Accurate stepping on a narrow path: mechanics, EMG, and motor cortex activity in the cat. *Journal of neurophysiology*, *114*(5), 2682–2702. https://doi.org/10.1152/jn.00510.2014

Freeman A. W. (2021) A model for the origin of motion direction selectivity in visual cortex. *The Journal of neuroscience 41*(1), 89–102. https://doi.org/10.1523/JNEUROSCI.1362-20.2020

Frenkel, M. Y., Sawtell, N. B., Diogo, A. C., Yoon, B., Neve, R. L., & Bear, M. F. (2006) Instructive effect of visual experience in mouse visual cortex. *Neuron*, *51*(3), 339–349. https://doi.org/10.1016/j.neuron.2006.06.026

Frostig, R. D., & Chen-Bee, C. H. (2009) Visualizing Adult Cortical Plasticity Using Intrinsic Signal Optical Imaging. In R. D. Frostig (Ed.), *In Vivo Optical Imaging of Brain Function*. (2nd ed.). CRC Press/Taylor & Francis.

Frostig, R. D., Lieke, E. E., Ts'o, D. Y., & Grinvald, A. (1990) Cortical functional architecture and local coupling between neuronal activity and the microcirculation revealed by in vivo high-resolution optical imaging of intrinsic signals. *Proceedings of the National Academy of Sciences of the United States of America*, *87*(16), 6082–6086. https://doi.org/10.1073/pnas.87.16.6082

Frostig R. D. (2006) Functional organization and plasticity in the adult rat barrel cortex: moving out-of-the-box. *Current opinion in neurobiology*, *16*(4), 445–450. https://doi.org/10.1016/j.conb.2006.06.001

Frostig, R. D., & Chen-Bee, C. H. (2009) Visualizing Adult Cortical Plasticity Using Intrinsic Signal Optical Imaging. In R. D. Frostig (Ed.), *In Vivo Optical Imaging of Brain Function*. (2nd ed.). CRC Press/Taylor & Francis.

Fröhlich, F., & McCormick, D. A. (2010) Endogenous electric fields may guide neocortical network activity. *Neuron*, *67*(1), 129–143. https://doi.org/10.1016/j.neuron.2010.06.005

Gonzalo Cogno, S., & Mato, G. (2015) The effect of synaptic plasticity on orientation selectivity in a balanced model of primary visual cortex. *Frontiers in neural circuits*, *9*, 42. https://doi.org/10.3389/fncir.2015.00042

Grinvald, A., Lieke, E., Frostig, R. D., Gilbert, C. D., & Wiesel, T. N. (1986) Functional architecture of cortex revealed by optical imaging of intrinsic signals. *Nature*, *324*(6095), 361–364. https://doi.org/10.1038/324361a0

Grinvald, A., Shoham D., Shmuel A., Glaser D., Vanzetta I., Shtoyerman E., Slovin H., Wijnbergen C., Hildesheim R. & Arieli A. (1999) In-vivo Optical Imaging of Cortical Architecture and Dynamics. In: Windhorst, U., Johansson, H. (eds) Modern Techniques in Neuroscience Research. Springer, Berlin, Heidelberg. https://doi.org/10.1007/978-3-642-58552-4_34

Heimel, J. A., Hartman, R. J., Hermans, J. M., & Levelt, C. N. (2007) Screening mouse vision with intrinsic signal optical imaging. *The European journal of neuroscience*, *25*(3), 795–804. https://doi.org/10.1111/j.1460-9568.2007.05333.x

Heindorf, M., Arber, S., & Keller, G. B. (2018) Mouse motor cortex coordinates the behavioral response to unpredicted sensory feedback. *Neuron*, *99*(5), 1040–1054.e5. https://doi.org/10.1016/j.neuron.2018.07.046

Hillman E. M. (2007) Optical brain imaging in vivo: techniques and applications from animal to man. *Journal of biomedical optics*, *12*(5), 051402. https://doi.org/10.1117/1.2789693

Hong, K. S., & Zafar, A. (2018) Existence of Initial Dip for BCI: An Illusion or Reality. *Frontiers in neurorobotics*, *12*, 69. https://doi.org/10.3389/fnbot.2018.00069

Hong, S. Z., Huang, S., Severin, D., & Kirkwood, A. (2020) Pull-push neuromodulation of cortical plasticity enables rapid bi-directional shifts in ocular dominance. *eLife*, *9*, e54455. https://doi.org/10.7554/eLife.54455

Hubel, D. H., & Wiesel, T. N. (1962) Receptive fields, binocular interaction and functional architecture in the cat's visual cortex. *The Journal of physiology*, *160*(1), 106–154. https://doi.org/10.1113/jphysiol.1962.sp006837

Hübener M. (2003) Mouse visual cortex. *Current opinion in neurobiology*, *13*(4), 413–420. https://doi.org/10.1016/s0959-4388(03)00102-8

Ibbotson, M., & Jung, Y. J. (2020) Origins of functional organization in the visual cortex. *Frontiers in systems neuroscience*, *14*, 10. https://doi.org/10.3389/fnsys.2020.00010

Jaramillo, S., & Zador, A. M. (2014) Mice and rats achieve similar levels of performance in an adaptive decision-making task. *Frontiers in systems neuroscience*, *8*, 173. https://doi.org/10.3389/fnsys.2014.00173

Jia, X., Siegle, J. H., Durand, S., Heller, G., Ramirez, T. K., Koch, C., & Olsen, S. R. (2022) Multiregional module-based signal transmission in mouse visual cortex. *Neuron*, *110*(9), 1585–1598.e9. https://doi.org/10.1016/j.neuron.2022.01.027

Jones, M. S., & Barth, D. S. (1999) Spatiotemporal organization of fast (>200 Hz) electrical oscillations in rat Vibrissa/Barrel cortex. *Journal of neurophysiology*, *82*(3), 1599–1609. https://doi.org/10.1152/jn.1999.82.3.1599

Kalatsky, V. A., & Stryker, M. P. (2003) New paradigm for optical imaging: temporally encoded maps of intrinsic signal. *Neuron*, *38*(4), 529–545. https://doi.org/10.1016/s0896-6273(03)00286-1

Kondo, S., Takashi Y., & Kenichi O.. (2016) Mixed functional microarchitectures for orientation selectivity in the mouse primary visual cortex. *Nature Communications* 7: 1–16. https://doi.org/10.1038/ncomms13210

Kreile, A. K., Bonhoeffer, T., & Hübener, M. (2011) Altered visual experience induces instructive changes of orientation preference in mouse visual cortex. *The Journal of neuroscience 31*(39), 13911–13920. https://doi.org/10.1523/JNEUROSCI.2143-11.2011

Laberge, D., & Kasevich, R. S. (2017) Neuroelectric tuning of cortical oscillations by apical dendrites in loop circuits. Frontiers in Systems Neuroscience, 11(June), 1–23. https://doi.org/10.3389/fnsys.2017.00037

Li, B., Peterson, M. R., & Freeman, R. D. (2003) Oblique effect: a neural basis in the visual cortex. *Journal of neurophysiology*, *90*(1), 204–217. https://doi.org/10.1152/jn.00954.2002

Lien, A. D., & Scanziani, M. (2013) Tuned thalamic excitation is amplified by visual cortical circuits. *Nature neuroscience*, *16*(9), 1315–1323. https://doi.org/10.1038/nn.3488

Lu, H. D., Chen, G., Cai, J., & Roe, A. W. (2017) Intrinsic signal optical imaging of visual brain activity: Tracking of fast cortical dynamics. *NeuroImage*, *148*, 160–168. https://doi.org/10.1016/j.neuroimage.2017.01.006

Malonek, D., & Grinvald, A. (1996) Interactions between electrical activity and cortical microcirculation revealed by imaging spectroscopy: implications for functional brain mapping. *Science (New York, N.Y.)*, *272*(5261), 551–554. https://doi.org/10.1126/science.272.5261.551

Mangini, N. J., & Pearlman, A. L. (1980) Laminar distribution of receptive field properties in the primary visual cortex of the mouse. *The Journal of comparative neurology*, *193*(1), 203–222. https://doi.org/10.1002/cne.901930114

Métin, C., Godement, P., & Imbert, M. (1988) The primary visual cortex in the mouse: receptive field properties and functional organization. *Experimental brain research*, *69*(3), 594–612. https://doi.org/10.1007/BF00247312

Morone K.A., Neimat J.S, Roe A.W. & Friedman R.M. (2017) Review of functional and clinical relevance of intrinsic signal optical imaging in human brain mapping. *Neurophotonics*, *4*(3), 031220. https://doi.org/10.1117/1.NPh.4.3.031220

Murty, D. V. P. S., Shirhatti, V., Ravishankar, P., & Ray, S. (2018) Large visual stimuli induce two distinct gamma oscillations in primate visual cortex. *The Journal of neuroscience: the official journal of the Society for Neuroscience*, *38*(11), 2730–2744. https://doi.org/10.1523/JNEUROSCI.2270-17.2017

Niell, C. M., & Stryker, M. P. (2008) Highly selective receptive fields in mouse visual cortex. *The Journal of neuroscience: the official journal of the Society for Neuroscience*, *28*(30), 7520–7536. https://doi.org/10.1523/JNEUROSCI.0623-08.2008

Niell, C. M., & Stryker, M. P. (2010) Modulation of visual responses by behavioral state in mouse visual cortex. *Neuron*, *65*(4), 472–479. https://doi.org/10.1016/j.neuron.2010.01.033

Ohki, K., & Reid, R. C. (2007) Specificity and randomness in the visual cortex. *Current opinion in neurobiology*, *17*(4), 401–407. https://doi.org/10.1016/j.conb.2007.07.007

Parker, P. R. L., Brown, M. A., Smear, M. C., & Niell, C. M. (2020) Movement-related signals in sensory areas: roles in natural behavior. *Trends in neurosciences*, *43*(8), 581–595. https://doi.org/10.1016/j.tins.2020.05.005

Perry, C. J., & Fallah, M. (2014) Feature integration and object representations along the dorsal stream visual hierarchy. *Frontiers in computational neuroscience*, *8*(84), https://doi.org/10.3389/fncom.2014.00084

Pielecka-Fortuna, J., Kalogeraki, E., Fortuna, M. G., & Löwel, S. (2015) Optimal level activity of matrix metalloproteinases is critical for adult visual plasticity in the healthy and stroke-affected brain. *eLife*, *5*, e11290. https://doi.org/10.7554/eLife.11290

Polack, P. O., & Contreras, D. (2012) Long-range parallel processing and local recurrent activity in the visual cortex of the mouse. *The Journal of neuroscience: the official journal of the Society for Neuroscience*, *32*(32), 11120–11131. https://doi.org/10.1523/JNEUROSCI.6304-11.2012

Raichle, M. E., Grubb, R. L., Jr, Gado, M. H., Eichling, J. O., & Ter-Pogossian, M. M. (1976) Correlation between regional cerebral blood flow and oxidative metabolism. In vivo studies in man. *Archives of neurology*, *33*(8), 523–526. https://doi.org/10.1001/archneur.1976.00500080001001

Rao, S. C., Rainer, G., & Miller, E. K. (1997) Integration of what and where in the primate prefrontal cortex. *Science (New York, N.Y.)*, *276*(5313), 821–824. https://doi.org/10.1126/science.276.5313.821

Rector, D. M., Carter, K. M., Volegov, P. L., & George, J. S. (2005) Spatio-temporal mapping of rat whisker barrels with fast scattered light signals. *NeuroImage*, *26*(2), 619–627. https://doi.org/10.1016/j.neuroimage.2005.02.030

Rector, D. M., Rogers, R. F., Schwaber, J. S., Harper, R. M., & George, J. S. (2001) Scattered-light imaging in vivo tracks fast and slow processes of neurophysiological activation. *NeuroImage*, *14*(5), 977–994. https://doi.org/10.1006/nimg.2001.0897

Rector, D. M., Rogers, R. F., & George, J. S. (1999) A focusing image probe for assessing neural activity in vivo. *Journal of neuroscience methods*, *91*(1-2), 135–145. https://doi.org/10.1016/s0165-0270(99)00088-6

Rector, D. M., Yao, X., Harper, R. M., & George, J. S. (2009) In Vivo Observations of Rapid Scattered Light Changes Associated with Neurophysiological Activity. In R. D. Frostig (Ed.), *In Vivo Optical Imaging of Brain Function*. (2nd ed.). CRC Press/Taylor & Francis.

Ringach, D. L., Mineault, P. J., Tring, E., Olivas, N. D., Garcia-Junco-Clemente, P., & Trachtenberg, J. T. (2016) Spatial clustering of tuning in mouse primary visual cortex. *Nature Communications*, *7*, 1–9. https://doi.org/10.1038/ncomms12270

Rochefort, N. L., Narushima, M., Grienberger, C., Marandi, N., Hill, D. N., & Konnerth, A. (2011) Development of direction selectivity in mouse cortical neurons. *Neuron*, *71*(3), 425–432. https://doi.org/10.1016/j.neuron.2011.06.013

Rossi, L. F., Harris, K. D., & Carandini, M. (2020) Spatial connectivity matches direction selectivity in visual cortex. *Nature*, *588*(7839), 648–652. https://doi.org/10.1038/s41586-020-2894-4

Roth, M. M., Helmchen, F., & Kampa, B. M. (2012) Distinct functional properties of primary and posteromedial visual area of mouse neocortex. *The Journal of neuroscience 32*(28), 9716–9726. https://doi.org/10.1523/JNEUROSCI.0110-12.2012

Salinas, K. J., Figueroa Velez, D. X., Zeitoun, J. H., Kim, H., & Gandhi, S. P. (2017) Contralateral bias of high spatial frequency tuning and cardinal direction selectivity in mouse visual cortex. *The Journal of neuroscience 37*(42), 10125–10138. https://doi.org/10.1523/JNEUROSCI.1484-17.2017

Schindelin, J., Arganda-Carreras, I., Frise, E., Kaynig, V., Longair, M., Pietzsch, T., Preibisch, S., Rueden, C., Saalfeld, S., Schmid, B., Tinevez, J. Y., White, D. J., Hartenstein, V., Eliceiri, K., Tomancak, P., & Cardona, A. (2012) Fiji: an open-source platform for biological-image analysis. *Nature methods*, *9*(7), 676–682. https://doi.org/10.1038/nmeth.2019

Scholl, B., Pattadkal, J. J., & Priebe, N. J. (2017) Binocular disparity selectivity weakened after monocular deprivation in mouse V1. *The Journal of neuroscience 37*(27), 6517–6526. https://doi.org/10.1523/JNEUROSCI.1193-16.2017

Scholl, B., Tepohl, C., Ryan, M. A., Thomas, C. I., Kamasawa, N., & Fitzpatrick, D. (2022) A binocular synaptic network supports interocular response alignment in visual cortical neurons. *Neuron*, *110*(9), 1573–1584.e4. https://doi.org/10.1016/j.neuron.2022.01.023

Schuett, S., Bonhoeffer, T., & Hübener, M. (2002) Mapping retinotopic structure in mouse visual cortex with optical imaging. *Journal of Neuroscience*, *22*(15), 6549–6559. https://doi.org/10.1523/JNEUROSCI.22-15-06549.2002

Sintsov, M., Suchkov, D., Khazipov, R., & Minlebaev, M. (2017) Developmental changes in sensory-evoked optical intrinsic signals in the rat barrel cortex. *Frontiers in cellular neuroscience*, *11*, 392. https://doi.org/10.3389/fncel.2017.00392

Skyberg, R., Tanabe, S., & Cang, J. (2020) Two is greater than one: binocular visual experience drives cortical orientation map alignment. *Neuron*, *107*(2), 209–211. https://doi.org/10.1016/j.neuron.2020.06.029

Sohya, K., Kameyama, K., Yanagawa, Y., Obata, K., & Tsumoto, T. (2007) GABAergic neurons are less selective to stimulus orientation than excitatory neurons in layer II/III of visual cortex, as revealed by in vivo functional Ca2+ imaging in transgenic mice. *The Journal of neuroscience 27*(8), 2145–2149. https://doi.org/10.1523/JNEUROSCI.4641-06.2007

Straka, H., Simmers, J., & Chagnaud, B. P. (2018) A new perspective on predictive motor signaling. *Current biology: CB*, *28*(5), R232–R243. https://doi.org/10.1016/j.cub.2018.01.033

Tan, A. Y., Brown, B. D., Scholl, B., Mohanty, D., & Priebe, N. J. (2011) Orientation selectivity of synaptic input to neurons in mouse and cat primary visual cortex. *The Journal of neuroscience 31*(34), 12339–12350. https://doi.org/10.1523/JNEUROSCI.2039-11.2011

De Valois, R. L., Albrecht, D. G., & Thorell, L. G. (1982) Spatial frequency selectivity of cells in macaque visual cortex. *Vision research*, *22*(5), 545–559. https://doi.org/10.1016/0042-6989(82)90113-4

Wang, B. S., Sarnaik, R., & Cang, J. (2010) Critical period plasticity matches binocular orientation preference in the visual cortex. *Neuron*, *65*(2), 246–256. https://doi.org/10.1016/j.neuron.2010.01.002

Wagor, E., Mangini, N. J., & Pearlman, A. L. (1980) Retinotopic organization of striate and extrastriate visual cortex in the mouse. *The Journal of comparative neurology*, *193*(1), 187–202. https://doi.org/10.1002/cne.901930113

De Weerd, P., Vandenbussche, E., & Orban, G. A. (1990) Staircase procedure and constant stimuli method in cat psychophysics. *Behavioural brain research*, *40*(3), 201–214. https://doi.org/10.1016/0166-4328(90)90077-r

Weiler, S., Guggiana Nilo, D., Bonhoeffer, T., Hübener, M., Rose, T., & Scheuss, V. (2022) Orientation and direction tuning align with dendritic morphology and spatial connectivity in mouse visual cortex. *Current biology : CB*, *32*(8), 1743–1753.e7. https://doi.org/10.1016/j.cub.2022.02.048

Wood, J., Freemantle, N., King, M., & Nazareth, I. (2014) Trap of trends to statistical significance: likelihood of near significant P value becoming more significant with extra data. *BMJ (Clinical research ed.)*, *348*, g2215. https://doi.org/10.1136/bmj.g2215

Yang, C. F., Yu-Chih Chen, M., Chen, T. I., & Cheng, C. F. (2014) Dose-dependent effects of isoflurane on cardiovascular function in rats. *Tzu Chi Medical Journal, 26*(3), 119–122. https://doi.org/10.1016/j.tcmj.2014.07.005

Yao X. C. (2009) Intrinsic optical signal imaging of retinal activation. *Japanese journal of ophthalmology*, *53*(4), 327–333. https://doi.org/10.1007/s10384-009-0685-4

Yoshida, T., Ozawa, K., & Tanaka, S. (2012) Sensitivity profile for orientation selectivity in the visual cortex of goggle-reared mice. *PloS one*, *7*(7), e40630. https://doi.org/10.1371/journal.pone.0040630

Zack, G. W., Rogers, W. E., & Latt, S. A. (1977) Automatic measurement of sister chromatid exchange frequency. *The journal of histochemistry and cytochemistry: official journal of the Histochemistry Society*, *25*(7), 741–753. https://doi.org/10.1177/25.7.70454

Zepeda, A., Arias, C., & Sengpiel, F. (2004) Optical imaging of intrinsic signals: recent developments in the methodology and its applications. *Journal of neuroscience methods*, *136*(1), 1–21. https://doi.org/10.1016/j.jneumeth.2004.02.025

Zhao, X., Chen, H., Liu, X., & Cang, J. (2013) Orientation-selective responses in the mouse lateral geniculate nucleus. *The Journal of neuroscience 33*(31), 12751–12763. https://doi.org/10.1523/JNEUROSCI.0095-13.2013

Zhang, Q.F., Li, H., Chen, M., Guo, A., Wen, Y., & Poo, M. (2018) Functional organization of intrinsic and feedback presynaptic inputs in the primary visual cortex. *Proceedings of the National Academy of Sciences of the United States of America, 115*(22), E5174–E5182. https://doi.org/10.1073/pnas.1719711115

Zhang, X., Yi, H., Bai, W., & Tian, X. (2015) Dynamic trajectory of multiple single-unit activity during working memory task in rats. *Frontiers in computational neuroscience*, *9*, 117. https://doi.org/10.3389/fncom.2015.00117

SUPPLEMENTARY MATERIALS

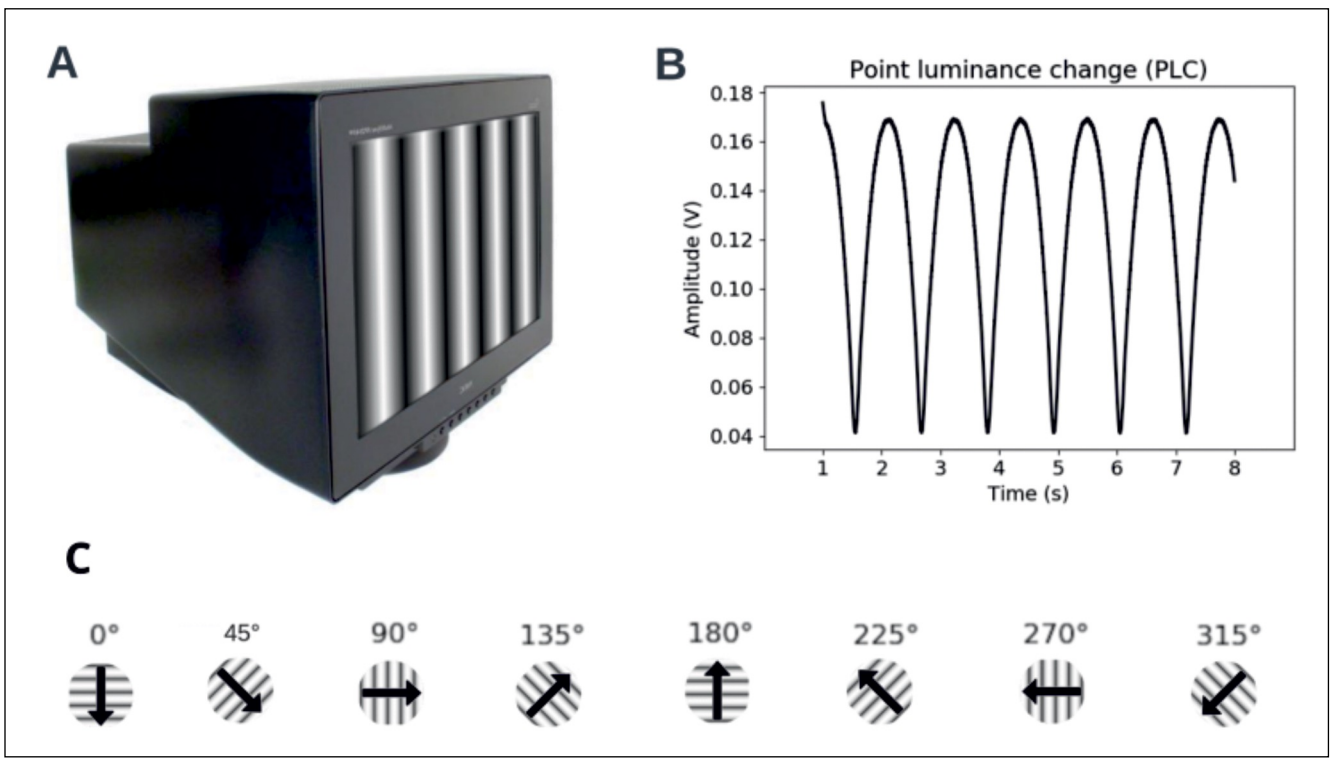

Supplementary Fig. 1. PLC recording. A. An example of sinusoidal grating moved along the horizontal orientation of 270° (←). B. During the movement of the grating photodiode placed at the center of the screen, the PLC signal was recorded with the main oscillatory component of 0.8571 Hz. C. The visual stimuli consisted of black-and-white gratings of sinusoidal luminosity displayed on the whole screen and moving in one direction perpendicular to eight different orientations: 0° moved from top to bottom, 45° from top left corner to bottom right corner, 90° from left to right, 135° from bottom left corner to top right corner, 180° from bottom to top, 225° from bottom right corner to top left corner, 270° from left to right, 315° from top right corner to bottom left corner.

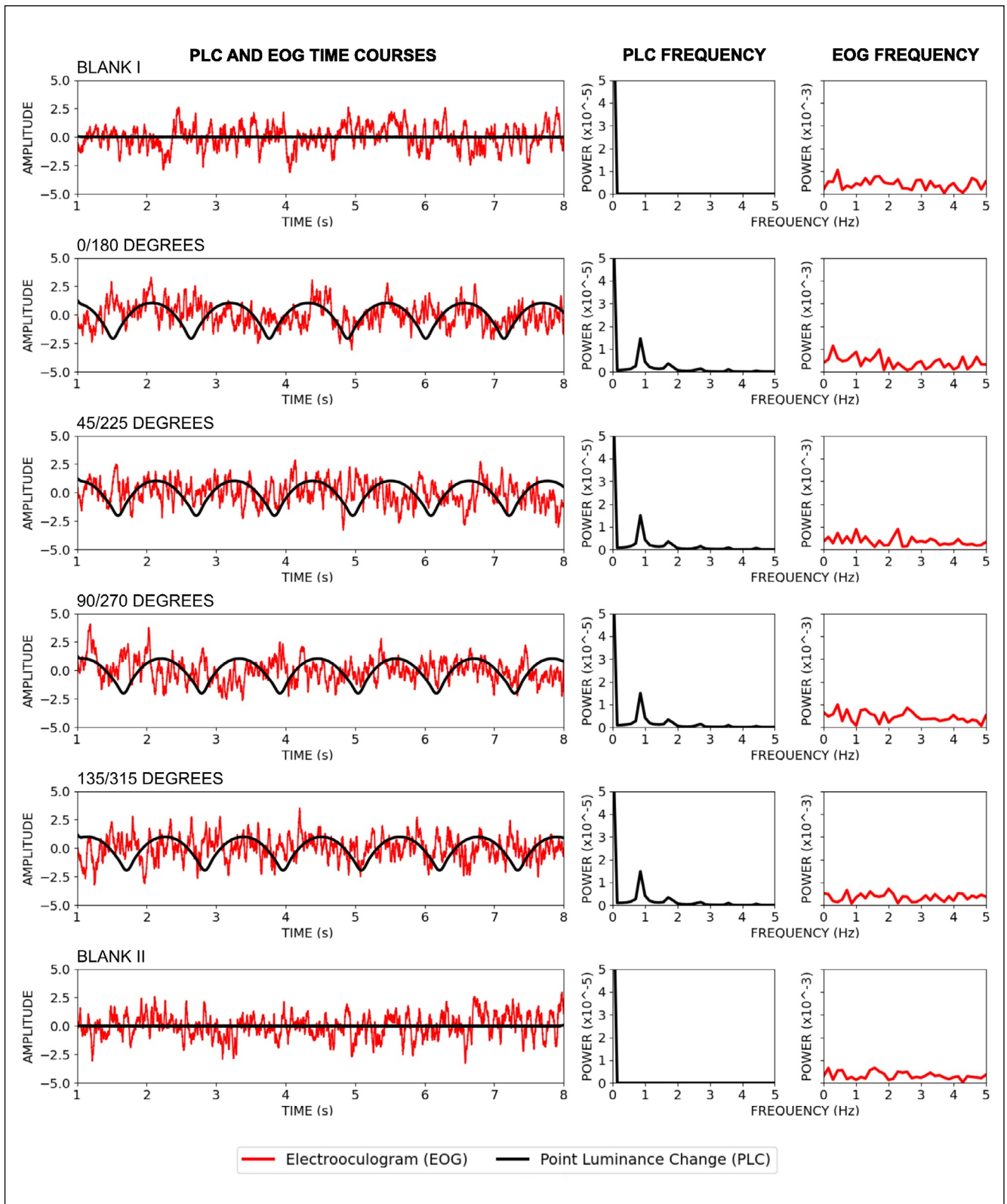

Supplementary Fig. 2. Time courses and frequency distributions of electrooculographic (EOG) and PLC signals. The figure provides a summary of the time courses (first column) and frequency distributions (second and third columns) for EOG (red line) and PLC (black line) signals recorded under six experimental conditions: BLANK I, 0°/180°, 45°/225°, 90°/270°, 135°/315°, and BLANK II. EOG signal recordings were obtained from a single mouse, while PLC signal recordings were taken from a photodiode placed in the center of the screen.